DOE/JPL 954355/79-1
Distribution Category UC-63

Mobil Tyco Solar Energy Corporation
16 Hickory Drive
Waltham, Massachusetts 02154

LARGE AREA SILICON SHEET BY EFG

Program Manager: F.V. Wald

First Quarterly Report - Subcontract No. 954355

Covering Period: January 1, 1979 - March 31, 1979

April 15, 1979

"The JPL Low-Cost Silicon Solar Array Project is sponsored by the Department of Energy and forms part of the Solar Photovoltaic Conversion Program to initiate a major effort toward the development of low-cost solar arrays. This work was performed for the Jet Propulsion Laboratory, California Institute of Technology by agreement between NASA and DOE."

ABSTRACT

In growth station JPL No. 1 the work during this quarter centered around trying to evaluate any influences on ribbon quality which might be caused by various materials of construction which are used in the growth furnace. At the present level of ribbon quality, which has produced 8.5% to 9.5% efficient solar cells, no particular influence of any furnace part was detected. The experiments rather led to the suspicion that the general environment and the somewhat unoptimized materials handling procedures might be responsible for the current variations in ribbon quality and that, therefore, continuous work with this furnace under rather more stringent environmental conditions and operating procedures could perhaps improve materials quality to some extent. The work on Machine 3A (the multiple furnace) was continued in this quarter with two multiple growth runs being performed. In these runs, the melt replenishment system performed poorly and extensive modifications to it have been designed to make reliable melt feeding for five ribbon growth possible. Although in the first quality assessment runs ever performed with the melt replenishment system diffusion lengths nearly as great as those found in non-melt replenished runs were found, we have not yet apparently identified all the factors affecting SiC density in ribbons grown from this large volume furnace. Thus, cell performance on multiple ribbon has not yet been demonstrated. The 10 cm width growth cartridge was also completely constructed during this quarter and will be checked out as soon as the multiple runs have been completed.

We also report on certain new characterization techniques for wide ribbons as well as on stress measurements and growth dynamics experiments, the latter being a necessary precursor to the design of automatic control techniques.

Table of Contents

List of Figures

List of Tables

I. INTRODUCTION

At the beginning of the fiscal year on which this document reports, it was well established that EFG material, in spite of its imperfect nature, is quite capable of producing large area (2.5 x 10 cm^2) solar cells with efficiencies of at least 12%. Indeed, the discussion of whether small area cells of higher efficiency could conceivably be prepared from some of the material, had already been shifting to the question of defining the influence of particular defects on the overall yield of cells prepared from whole multiple meter lengths of ribbon, and attempts to prepare single cells with optimized properties were de-emphasized.

Instead, under this contract the focus shifted to considering even larger cells (5 x 10 cm^2 and 7.5 x 7.5 cm^2) prepared from 5 cm and 7.5 cm wide ribbon, grown under conditions which would make high rate multiple ribbon growth a practical reality. The characterization task, therefore, took more and more of an interest in questions related to uniformity of properties over very large cell areas and within long ribbons, instead of concerning itself with the top performance of selected small ribbon areas.

Thus, the program in its philosophy shifted to engineering research, i.e., answering questions related to specific machine design elements; the ribbon quality to be expected from growth stations built in certain ways and using particular materials of construction, and the relations between silicon ribbon quality and productivity; i.e., such questions as to how speed and width affect the ribbon properties both from a mechanical (flatness, thickness uniformity, etc.) and solid-state (in the end, solar cell efficiency) standpoint.

Overall, we believe that this programmatic approach has been successful and that a realistic engineering concept has been proven which will allow the achievement of high ribbon productivity along with good ribbon quality and thus low solar cell blank cost. Specifically, major achieve-

ments of the program which support this statement are:

1. The soundness of the engineering concepts has been demonstrated by the achievement of multiple (five) ribbon growth for periods up to 20 hours.

2. Significantly improved single ribbon equipment using a cartridge (Machine 17) has been constructed on schedule this year. It provides unique capabilities for studying and understanding the growth process itself as well as a simple basic concept for automatic feedback control.

3. The work on JPL Machine No. 1 (MTSEC No. 18) has led to the design of highly reliable growth cartridges in which experiments of 7.5 cm wide growth can be conducted in a reproducible manner, i.e., when one sets out to grow a ribbon, one can actually grow as much as a full crucible allows every time. During the last three months, this equipment operated on a regular schedule of two one-day runs per week, without any significant parts failure.

4. The introduction of the so-called "mini cold shoe" represents a major advance in reliable cartridge design.

5. A concept that had been proposed for some time, namely to use specific interface shaping to improve material properties of wide ribbon, has finally been reduced to practicability by the use of displaced dies. This has led to solar cells (in sizes of 2.5 x 10 cm^2, 2.5 x 7.5 cm^2, and 7.5 x 7.5 cm^2) grown from a reliable, practical cartridge system which have average efficiencies of over 9% in random lots of ~10 pieces. Most importantly, the material is indeed asymmetrical as predicted, not only with respect to solar cell efficiency but also with respect to silicon carbide density.

Thus, enough understanding of the effects has been gained to make further advances in this area quite likely so that the solar cell efficiency in these large ribbon cells is expected to reach similar averages which are now obtained in cells made from smaller ribbons.

6. Detailed studies of the effect of the gaseous environment in an EFG furnace have led to the discovery that growth stability can be significantly enhanced and SiC density can be greatly reduced by proper atmosphere control.

However, before final production machine prototype design can begin, the various approaches which have been derived need still to be optimized and made ready for fully automatic operation at high growth rates, a fact

that becomes clearly apparent from the detailed discussions in the text that follows. In particular, the main hurdle toward higher growth rates, namely the buckling that produces unacceptable, non-flat ribbon, has to be overcome and the approaches toward higher cell efficiencies have to be refined so that they are more effective and can be combined with high growth rates (> 5 cm/min).

Experiments which generate the needed basic facts in these areas can, however, be conducted now in an optimum way, since both direct observational tools (Machine 17) and sufficient basic understanding of the details of the growth process are available. We are thus confident that the final prototype design of a ribbon production machine could begin within a year.

II. WORK ON CRYSTAL GROWTH STATION NO. 1 by J.P. Kalejs

A. Overview

The study of the influence of furnace and cartridge materials of construction and component design on ribbon quality has been continued in JPL No. 1 in a third series of clean runs. The purpose of quality baseline runs has been threefold: (i) to evaluate the effect of the replacement of molybdenum shielding in the cartridge and the main zone with graphite, (ii) to compare the quality of ribbon grown with and without the cold shoe over the growth speed range from 2 to 3 cm/min; and (iii) to evaluate die design influence, with respect to melt flow geometry and die top displacement, on material quality. The quality baseline studies have been done on 5.5 cm wide ribbon grown in the 7.5 cm cartridge system. Investigation of growth stability with deliberately introduced asymmetries in the die top environment has been carried out with 7.5 cm wide ribbon in parallel with the quality baseline runs. The main emphasis here has been on examining the effects of cold shoe asymmetry on growth stability and material quality.

Characterization of the material grown in this most recent series has been limited to date to the measurement of diffusion lengths on as-grown material with the SPV method. Diffusion lengths in the 5.5 cm wide ribbon are comparable to those reported for 7.5 cm wide ribbon in the runs which produced solar cells with the best efficiencies, in the range from 9% to 10% (AM1 and AR coated).[1] Within the constraints imposed by SPV diffusion lengths as a criterion by which to judge material quality (as discussed in Section IV), the ribbon quality has been found to be relatively insensitive to the presence or absence of the cold shoe, to the substitution of graphite for molybdenum as the construction material for certain furnace and cartridge components, and to variations in the dimensions of the die capillary.

B. Experimental

A new series of clean runs designed to examine in more detail the effect of a number of variables on material quality was initiated with run 18-117. A summary of the runs carried out in this quarter is given in Table I. Provisions were made to allow interchange of the molybdenum die-top shield in the cartridge and the entire main zone molybdenum insulation assembly with components made of graphite. Together these changes remove a substantial part of the molybdenum from the growth system. In those runs in which the cold shoe was removed, the molybdenum afterheater shields were also taken out. The only molybdenum then remaining was that contained in the cartridge and main zone heater power feed rods, and gas flow tubes.

The introduction of a new design of die to aid in quality studies has been coupled with the initiation of growth of 5.5 cm wide ribbon. Otherwise, the 7.5 cm cartridge remained unchanged for the quality baseline runs, with the exceptions noted in Table I. A modified 7.5 cm wide die, with notches at appropriate locations in the die top to aid narrower ribbon growth, was introduced in run 18-118. Growth was less stable than for full-width ribbon, but adequate. No deliberate attempt was made to optimize growth conditions at this stage because the main purpose of going to narrower ribbon was to expedite material quality evaluation.

The new open channel die predominantly used in material quality studies in this series of clean runs in shown in Fig. 1. One of the problems with the central five-capillary die, which has proven to give the best material to date,[1] has been lack of reliability due to SiC particle growth in the capillaries. The new design attempts to alleviate this situation. The capillary is formed by the die-top slot and a single saw cut made into the die bottom, as shown in Fig. 1, which meet so as to form a constricted channel for melt flow. This geometry allows positioning of the constriction in the capillary channel closer to the growth interface than was possible with the design of saw cut die described in a previous report,[2] while also providing flexibility for varying the constriction width.

1. Asymmetric Cold Shoe

Six runs in the current series were utilized for the purpose of investigating the effect of cold shoe asymmetry on growth stability and material quality. Earlier experiments had shown that asymmetries in such cartridge components as the face heater and die-top shield did not

Table I. JPL No. 1 Run and Ribbon Data. All-Molybdenum Cold Shoe with 0.32 cm Spacing, Graphite Main Zone Insulation and Die Top Shield Used in all Quality Baseline Runs, Except as Noted.

Run No.	Speed (cm/min)	Length (m)	Comments
18-117	2.0 - 3.2	2 4	First run of third clean series. "All-graphite" system with new main zone graphite fiberform insulation, and graphite die-top shield. Standard 0.012 cm displacement, central five-capillary die.
18-118	2.5 - 3.0	1.5	Repeat of 18-117 with die modified for 5.5 cm wide ribbon growth. Operator training.
18-119	2.3 - 2.5	1.7	Repeat of 18-118 with non-displaced die. Return to use of single 0.15 cm thick molybdenum die-top shield.
18-120	3.2 - 4.0	1.7	First test of asymmetric heat removal elements (0.08 cm displacement) and 0.010 cm displacement die. Growth conditions reasonable.
18-121	2.0 - 2.7	7.2	First test of 2.5 cm wide central channel die, 0.012 cm displacement, 5.5 cm wide ribbon graphite crucible baseline run.
18-122	2.5 - 3.6	0.5	Repeat of run 18-120 with interchanged cold shoe and die displacements. Growth conditions very poor.
18-123	2.2 - 2.8	4.4	First quality baseline run with quartz crucible, 2.5 cm (B dimension) open channel die, 0.012 cm displacement. Melt temperature deliberately varied.
18-124	-	-	Repeat of run 18-120 configuration with 0.10 cm displacement cold shoe and 0.025 cm displacement die. Growth impossible due to thermal imbalances at die top.
18-125	1.8 - 2.3	5.0	First quality baseline run with 5 cm (B dimension) open channel die, 0.012 cm displacement.
18-126	2.0 - 3.0	3.2	Repeat of run 18-123, melt temperature deliberately varied.
18-127	2.9 - 3.8	1.3	0.10 cm displaced cold shoes with a regular (non-displaced) die, 2.5 cm channel. Undoped melt. Growth reasonable. No observable meniscus height asymmetry or SiC particle asymmetry.

Table I (continued)

Run No	Speed (cm/min)	Length (m)	Comments
18-128	-	-	Repeat of run 18-121. Cold shoe rupture and water flood in main zone. No growth possible.
18-129	1.8 - 2.5	4.7	First quality baseline run in clean series with molybdenum main zone shielding and without cold shoe. 2.5 cm open channel die, 0.012 cm displacement (same as run 18-121).
18-130	1.8 - 2.3	3.7	Repeat of run 18-129 with 5 cm open channel displaced die.
18-131	-	-	Test of 0.125 cm side channel die. Growth not possible due to thermal imbalance and poor melt feed conditions.
18-132	2.8 - 3.0	3.2	Test of 0.64 cm side channel die. Growth difficult to initiate. Reasonable stability. All-molybdenum cold shoe, 0.24 cm opening.
18-133	1.8 - 2.5	5.7	First quality baseline run without cold shoe and with all-graphite system (see run 18-117). 2.5 cm central channel die, 0.025 cm wide top slot with 0.008 cm displacement.
18-134	1.9 - 2.8	1.6	First run with cooling blocks and heat removal elements removed from one ribbon face. Regular flat die without displacement. Growth conditions reasonable Undoped melt. Dendritic growth at ribbon edges.
18-135	1.5 - 2.0	3.4	Repeat of 18-133 with 0.75 cm open channel die, 0.035 top slot and 0.012 cm displacement.
18-136	2.3	0.2	Repeat of run 18-134 with a displaced die; 4.5 cm channel, 0.05 cm top slot, and 0.012 cm displacement. Growth limited by puller malfunction. Initial growth reasonable.

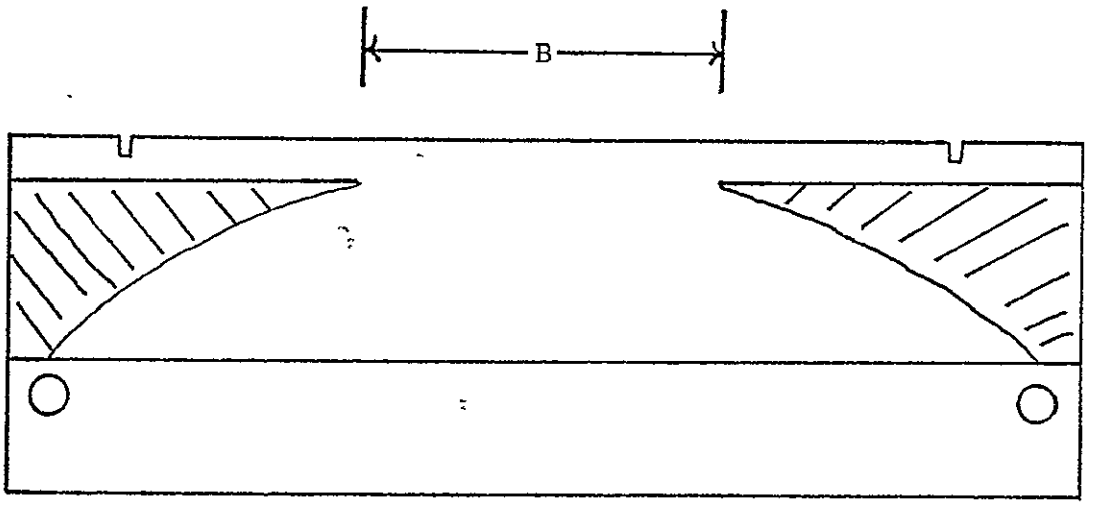

Fig. 1. Open channel die cross section. Constriction dimension across ribbon width is denoted by B. The die top notches fix width for 5.5 cm wide ribbon growth.

exert a first-order effect on growth ease or material quality. These experiments were extended in this present series to involve cold shoe modifications, which culminated in two runs (18-134 and 18-136) with the cooling block from one face of the ribbon removed entirely from the cartridge.

Growth of ribbon with several displaced cold shoe and die combinations (runs 18-120, 18-122, 18-124 and 18-126) generally did not lead to improved growth stability at the large die displacements used (0.025 cm).[3] Variations in growth conditions from run to run were not predictable on the basis of expected changes arising from the deliberately introduced cold shoe modifications, and were attributed to perturbations in the die-top thermal environment by unassociated causes. This viewpoint was strengthened in the two runs with the cold shoe removed from one face of the ribbon. Run 18-134 utilized a flat, non-displaced die; a standard 0.012 cm displaced die was used in run 18-136, with the high side of the die away from the cold shoe. Growth conditions were considered reasonable in both runs, although only limited growth was possible in run 18-136 due to a malfunction in the stroke puller. The absence of the cold shoe across one face of the ribbon did not produce a measurable change in the meniscus height from face to face in run 18-134. The height was measured with a reticled lens in the microscope, the error in the measurement was estimated to be about 0.005 cm on a meniscus height of 0.025 cm. Prominent interface shape deviations, arising from what appeared to be dendritic growth, were observed at each of the ribbon edges. These tended to make control of the ribbon edge position difficult, and were quite uncharacteristic of growth with symmetric cold shoes. Similar observations were not made in run 18-136 with the displaced die because of the early termination of the run.

2. Growth Without the Cold Shoe; Graphite vs. Molybdenum

The main effort in the quality baseline runs has been to obtain a comparison of material quality of ribbon grown with and without the cold shoe and with replacement of other molybdenum components with graphite over an overlapping growth speed range. The quality baseline runs from 18-117 to 18-126 utilized the regular all-molybdenum cold shoe. The growth speed was deliberately kept in the range from 2 to 3 cm/min. Runs were made both with graphite and molybdenum die-top shields. Starting with run 18-129, a changeover was made to a cartridge without a cold shoe. Because of a water flood in run 18-128, which required the graphite main

zone insulation to be re-baked, a return was made to molybdenum main zone insulation for the initial two runs without a cold shoe. New baked-out graphite main zone insulation was re-installed for the next two quality baseline runs without the cold shoe (runs 18-133 and 18-135).

Growth conditions with and without the cold shoe were not noticeably different over the lower speed range from 1.8 to 2.3 cm/min. However, above 2.5 cm/min growth in the cartridge without the cold shoe became more unstable. This is to be expected on the basis of heat transfer considerations because the speed for the given ribbon thickness is now approaching more closely the limiting growth speed of this system (estimated to be about 3.5 cm/min), at which a complete loss of stability is predicted to occur.

Growth conditions with the "all-graphite" system, including a graphite die-top shield and all-fiberform main zone insulation, were also not noticeably changed from those with the all-molybdenum insulation. The use of the graphite die-top shield in place of the molybdenum did appear to reduce the maximum speed capability of the system. This has been attributed to a reduction of the temperature gradient at the die top arising from the presence of the graphite shield, which appeared to lead to conditions where the die top was hotter than with a molybdenum shield of the same thickness.

3. Die Design Studies

All the quality baselines runs, with the exception of the first three, utilized dies of the design shown in Fig. 1. The width* of the die-top slot, the dimension "B" of the constriction in the melt flow channel, and the magnitude of the displacement were varied from run to run: the die-top slot width ranged from 0.025 cm to 0.050 cm; the constriction dimension was in the range from 0.75 cm to 5.0 cm; and the displacements went from 0.008 cm to 0.012 cm, with the smaller values for the narrower die-top slots.

Two variations of the side channel die used in the aluminum redistribution experiments described in an earlier report[1] were tried out in runs 18-131 and 18-132. Growth attempts with a 0.125 cm deep and 0.025 cm wide vertical capillary slot at each end of the die were not successful in run 18-131. The melt feed with this narrow channel appeared to be insufficient to supply the growth interface. Growth conditions were im-

*The dimension perpendicular to the plane of Fig. 1.

proved and acceptable with a 0.64 cm deep and 0.050 cm wide vertical channel at each die end in run 18-132. The findings in these trials imply that the minimum capillary slot area needed for a melt feed rate sufficient for growth of 7 cm wide ribbon at speeds of up to 3 cm/min is in the range from 6 x 10^{-3} cm^2 to 6 x 10^{-2} cm^2 for this die design.

C. Material Quality Considerations

Characterization of ribbon grown in the last series of clean runs is summarized in Section IV. Significant variations in SPV diffusion length have not been observed to accompany changes in furnace and cartridge materials of construction from molybdenum to graphite, removal of the cold shoe, or variations in die capillary geometry. In general, the range of SPV diffusion lengths and their distribution across the ribbon width in the case of the 5.5 cm ribbon are very similar to those already reported for 7.5 cm wide ribbon.[2] SPV diffusion lengths have shown a repeatable pattern with respect to the ribbon width for all the central channel die design variations used, in that consistently higher diffusion lengths are found over the central portions of the ribbon, and lower values at the ribbon edges. However, variations in the diffusion length magnitude from sample to sample within a run and from run to run have made it difficult to evaluate the influence of a specific parameter on the material quality solely on the basis of the available data.

Spreading resistance and four-point probe measurements taken on ribbon grown with side channel dies[1] from an aluminum-doped melt have shown aluminum is redistributed across the ribbon width as well as the thickness. The redistribution pattern across the width can be accounted for by a two-dimensional model of impurity transport. Redistribution of aluminum is also observed across the ribbon thickness; possible causes include deviations of the interface shape from an ideal planar profile and departures from ideal melt flow conditions. A specific profile shape across the ribbon thickness or a given distribution of shapes across the ribbon width from sample to sample was not consistently reproduced in the side channel die data. This diversity was taken to reflect a lack of reproducibility in local growth conditions, which also are a factor in determining the local interface shape. The experiments with the aluminum-doped melts and data are discussed in more detail in Section IV and Appendix 7.

The preliminary results from growth runs with the displaced cold shoe and the large displacement (0.025 cm) dies have been discouraging.

SPV diffusion lengths from these runs have consistently been depressed below the average levels found in the standard quality baseline runs. At present there is no explanation for this trend, and further characterization is in progress to look for explanations.

The present series of clean runs is to be completed after several more runs. The furnace will be cleaned and, along with the cartridges, reassembled with cleaned and re-baked components in preparation for a fourth series of clean runs. Several minor design modifications will be initiated and adherence made to more consistent operating procedures to attempt to reduce the possibility of impurity contamination during the series. To this effect, development work with displaced dies and asymmetric cold shoes will be temporarily interrupted in order to assist in the maintaining of a stricter operating regimen and allow runs to proceed on a more regular and uninterrupted basis.

III. MULTIPLE RIBBON FURNACE by B.H. Mackintosh

A. Background

Progress in calendar year 1978 on the multiple ribbon system culminated in four important points:

- Significant numbers of 50 cm^2 solar cells with AM1 efficiencies of 8 to 8½% were produced from material grown in this system, using a single-cartridge hot zone.

- A major improvement in long-term stability of growth was realized through control of atmosphere contamination and by refinement of temperature control and pulling subsystems. After being proven in single-ribbon operation, these modifications were installed on the other four growth stations.

- A new full-length hot zone incorporating many improvements over the previous unit with regard to cleanliness, reliability, and mechanical stability was constructed and was ready for testing.

B. Principal Outcomes of Work of First Quarter 1979

- The new furnace was tested and trimmed for temperature uniformity. Performance is very satisfactory and excellent reliability has been demonstrated to date.

- Growth performance of cartridges in new furnace is as good as in old furnaces — no changes were required.

- Ribbon grown using new furnace in single-cartridge quality assessment run showed diffusion lengths as high as best runs in short hot zone.

• The melt replenishment system performed poorly when first operated in the new furnace due to better thermal insulation of the latter unit. With minor changes, reliable melt feeding at a rate equivalent to growth of two ribbons was achieved, and more extensive modifications were designed to obtain five-ribbon melting rate.

• Two multiple growth runs were performed. The first, a shakedown run of new furnace and new cartridge control systems, saw four ribbons grown simultaneously for two hours. In the second, five-ribbon growth was maintained for two hours; only insufficient melt feeding rate foreshortened the run.

• In the first quality assessment run ever performed with the melt replenishment system, ribbon was grown with measured diffusion lengths nearly as great as non-replenished quality-assessment ribbon.

• Factors affecting silicon carbide particle density in ribbon grown from the system in its present condition have not yet been positively identified. In five of the seven single-cartridge runs, surface density of these inclusions was great enough to seriously impact cell performance; in the other two runs, particle densities were very low. A definite relationship was not seen between this phenomenon and experimental variation of procedures carried out to date.

C. Details of Ribbon Growth Work

Table II presents a summary of the growth runs performed during this quarter. During January, the new furnace hot zone was tested and qualified for ribbon growth in three stages. In the first stage, the most basic aspects of the unit such as adequacy of water-cooling provisions, ability of all parts to withstand thermally-induced stresses, resistance match of heating elements to power supply, etc., were tested. Temperatures were read along the length of the hot zone at the cartridge positions, and the slotting pattern of the heating elements was modified to provide a more nearly uniform distribution. In the second stage of testing the hot zone, the growth behavior of a cartridge in the thermal environment of the new furnace was tested (run 172). A difference in control settings for the die face and end heaters was predicted and it was expected that the shape of the end heaters might need to be re-optimized, but the cartridge performance was very similar to that in the old furnace and no changes were needed. The third phase of testing purported to evaluate the cleanliness of the new hot zone by measuring dif-

Table II. Ribbon Growth Runs of First Quarter 1979. Furnace 3A.

No.	Purposes	Quantity Grown (m)	Principal Findings
172	First growth in new hot zone (one cartridge). First use of melt replenisher since Jan. 1978.	7.0	Cartridge performance okay in new furnace. Melt replenisher heating power inadequate - difficulty with freezing charge rod to funnel. Heavy SiC on ribbon.
173	Test melt replenisher after minor modifications. Keep furnace airtight throughout run - attempt to minimize SiC.	5.2	Melt replenisher blocked up and flooded - no feeding. Growth was from precharged crucible. Heavy SiC on ribbon despite airtight system.
174	Test melt replenisher after additional minor modifications.	7.9	Melt replenisher worked well at ~3 gm/min. (Adequate for two-ribbon simultaneous growth.) Very stable growth but heavy SiC.
175	Ribbon quality assessment - non-replenished. Experiments with hot zone purge flows.	10.7	Good, stable growth. SiC particle density varied considerably - not clear what factors caused variation.
176	Repeat 175.	9.1	Good, stable growth. SiC particle density lower than in 175.
177	Multiple run with low replenishment rate.	31.2	Grew four ribbons together for two hours. One setup unusable due to electronic component failure. Multiple operation quite manageable due to improved long term stability of individual units.
178	Quality run - non-replenished. Test internal capillary die bottom. Experiments with furnace and cartridge purging gases.	7.0	Excellent stability and low SiC helium in cartridge found not to be needed.
179	Quality run with replenishment. Repeat experiments with system purging gases.	12.6	Excellent stability. Low SiC density despite removal of cartridge during run to replace die.
180	Multiple run with low replenishment rate.	57.6	Grew five ribbons at once for two hours. Duration of this growth limited only by replenishment rate. Heavy SiC first half of run - then cleared up.

fusion lengths in ribbon grown from it in single cartridge runs under ideal conditions. This was the purpose of runs 175, 176, and 178. In the first two of these, silicon carbide particle densities were high (generally 20 to 30 particles per 50 cm^2 cell blank) and diffusion length measurements were widely scattered, giving rise to low average values. In run 178, however, particle densities were generally below 3 per 50 cm^2 sample, and growth behavior during the run was very stable. This ribbon yielded an average of diffusion length measurements as high as the best of the averages of runs in the short hot zone in the fourth quarter of 1978.

Once the new furnace had been proven satisfactory in these respects, only the melt feeding system required evaluation and development work before multiple growth runs could be performed. This essential system element had been built in late 1977 and used in five growth runs, the last of which was five-ribbon run 16-107 in January 1978. While the melt feeding rate achieved in that initial period of use was adequate to keep up with the withdrawal of silicon at the low duty rate of multiple growth in run 107, it was recognized as deficient for continuous five-ribbon growth. Several design changes were made early in 1978, and a period of development work devoted to melt replenishment was planned for mid-1978. Not only was the unit to be developed for adequate melting rate, but the effects on ribbon electronic quality of both melt replenishment in general and of use of this particular piece of apparatus were to be studied. However, time did not permit this work to be carried out in calendar year 1978, and these matters were attended to in the work of the first quarter of 1979.

Whereas the change to the new hot zone did not affect performance of the growth cartridges, the melt feeder's operation was seriously degraded by the difference in insulation design between the old and new furnaces. As the new insulation system was designed to be more efficient and to better isolate the cartridges thermally from one another, less heat was supplied by the main heaters to the lower section of the melt feeder. In the first two runs in which it was used, heating of the melting funnel was so deficient that the charge rod froze to it and could not be remelted. Minor modifications were made, and by the end of the reporting period, satisfactory charge melting at a rate equivalent to continuous growth of two ribbons was attained. One single-cartridge and two multiple-cartridge runs were made with the melt feeder in this condition. A more extensive modification which is expected to result in fully ade-

quate feeding rate was designed, and parts were ordered to implement it.

An important result was obtained in this period when, for the first time, a quality-assessment run was made using the melt feeding system. Standard clean assembly procedures were followed, and the run, number 179, was uneventful, with excellent growth stability. This run followed closely in time the non-replenished quality-assessment run, number 178, for which setup and operating procedures were otherwise similar. Diffusion length measurements made on ribbon from these two runs, as reported in Section IV, suggest that the melt replenishment system does not have a serious negative impact on ribbon quality.

Within the constraint of the melt feeder limitations described above, two multiple growth runs were made. In the first of these, number 175, one of the cartridges was inoperable due to a defective power supply component, but simultaneous growth of four ribbons was maintained for two hours. This performance was good in light of the fact that four of the cartridges and related systems had not been used for ribbon growth since major renovations had been made. In the second multiple run, number 180, five ribbons were simultaneously grown for two hours and four were grown for over four hours; only the deficient melt replenishment rate prevented full multiple growth from continuing for a much longer period. After the crucible had been nearly emptied in this run, three of the ribbons were stopped so that growth of the remaining two could be observed for an additional four hours. An important observation related to silicon carbide particle densities stemmed from this extended period of continuous ribbon growth, as discussed below.

In these two multiple runs, the results of work in the past year on long-term stability were apparent. The typical length of time between required corrections per growth station permitted the operator to divide his time among the four stations without strain. Yield of full-width ribbon was 95% in the five-ribbon multiple run and over 97% in single-ribbon runs 176, 178, and 179.

The problem of high densities of silicon carbide inclusions in ribbon surfaces was the subject of several experiments made in the growth runs of the quarter. In some growth runs of the third and fourth quarters of 1978, ribbon was pulled, from displaced tip dies, with one face perfectly or practically clear of SiC particles. The experience of these runs led to a tentative conclusion that the ribbon surface carbide particles could be kept at low concentrations by keeping the concentration of reactive species in the furnace atmosphere at a sufficiently low

value. A combination of main furnace purge flow, venting technique, and cartridge purge flow was found which seemed to accomplish this end for a single cartridge operated in the short hot zone. When the new furnace was installed, new features were added to improve sealing around the cartridge openings.* Because of these new features and the different gas flow patterns in the larger furnace, we expected to have to learn these elements of operating procedure anew. However, the task of establishing procedure for control of entrance of air into the furnace turned out not to be straightforward, as the runs performed turned up contradictory evidence about the importance of keeping the furnace airtight. In single-cartridge, non-replenished runs 175, 176, and 178, the furnace was airtight in the usual sense (cartridge fully inserted throughout run; unused openings blocked off; high argon outflow rate). However, ribbon growth in the first two of these had silicon carbide particles on the "good" (high meniscus) side of >10 per 50 cm^2 sample. The third produced ribbon with low to moderate (<10 per 50 cm^2) particle densities. In contrast, run 179 entailed removal and replacement of the cartridge early in the run, after the silicon had been melted. In lieu of trap doors, a plate of graphite was placed over the opening after removal of the cartridge. In spite of the backstreaming occurring during this procedure, all ribbon grown in this run had low (<3 per 50 cm^2) silicon carbide particle density. The other occasion in this reporting period on which low-carbide ribbon was grown for sustained periods was the second half of multiple run 180. In the first half of this run, four and five ribbons were grown for four hours starting with a full (1000 gm) crucible charge. This charge was gradually depleted as the melt replenisher was supplying silicon at less than the rate of withdrawal of two cartridges. All ribbon from this run portion had high silicon carbide particle density. When growth was stopped in three cartridges halfway through the run, the heater settings and gas flows in these were left unchanged, but the set point of the main furnace was lowered by 60 degrees. Within an hour after this time, silicon carbide particle densities dropped almost to zero on both the ribbons which continued to grow. We do not conclude that the overheated crucible condition prevailing in the first half of

*A set of all-graphite, quarter-turn trap doors like those in Furnace 17 was designed for this furnace, but the first set was made with excessive clearances in the pneumatic actuators and was unreliable in operation. Replacement parts have not been procured.

this run was alone responsible for the high silicon carbide particle densities; in two of the single-cartridge runs of this period in which crucible temperature did not exceed 15 degrees above silicon's melting point, high silicon carbide particle densities nevertheless were present. We tentatively conclude instead that the dilution effect of feeding silicon into a carbon-rich melt in a graphite crucible was the primary cause of diminution of numbers of carbide particles. Our experience with continuous melt feeding is not yet extensive enough that we may state this conclusion with certainty or prescribe conditions and procedures which will yield low-carbide ribbon. The experiments done so far with crucible temperature, treatment of furnace between runs, start-up procedure, cartridge removal, and flushing gas flows have yielded ambiguous results. Additional experiments are currently in progress in this area. The reliable achievement of low-carbide growth seems to be the last stage to be reached to demonstrate the operation of this multiple ribbon system in accordance with its 1978 contract year goals for throughput and solar cell performance.

D. Construction of Cartridge for 10 cm Wide Ribbon

A 10 cm ribbon cartridge, as depicted in Figs. 2 and 3, was designed and built during this quarter. The cartridge is photographed inverted from its position of use; the end of the die which is immersed in silicon is seen protruding from the top.

While this cartridge is similar in layout and construction to previous 5 and 7.5 cm ribbon versions, numerous detail refinements have been made which will improve reliability and facilitate development work.

Furnace 3A will be modified to accept the 10 cm cartridge after two more multiple 5 cm ribbon runs have been made. The 5 cm demonstration phase will end and this conversion will be made by about the end of May. The goal of the first phase of cartridge development in Furnace 3A will be to demonstrate sustained 10 cm wide growth at a rate of 3 to 3.5 cm/minute. Once this performance has been achieved, Furnace 1 will be converted for further development of the 10 cm cartridge toward the growth rate goal of 6 cm/minute. Multiple Furnace 3A will eventually be outfitted with three 10 cm cartridges for multiple growth demonstration runs in mid-1980.

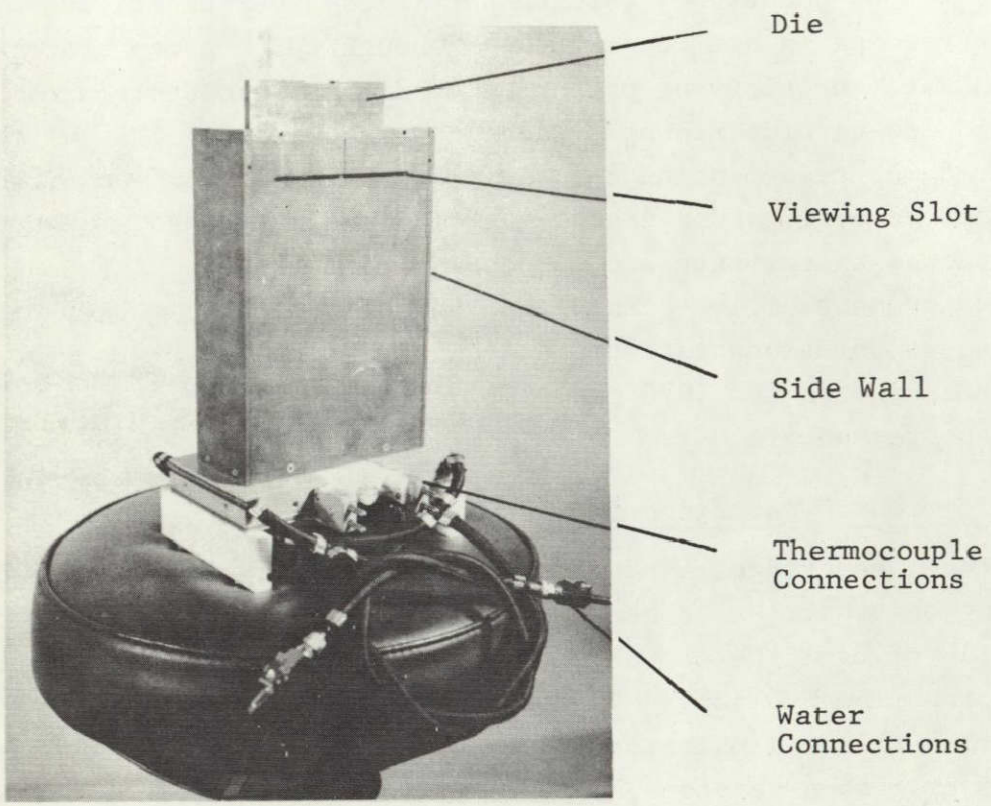

Fig. 2. 10 cm ribbon cartridge, complete.

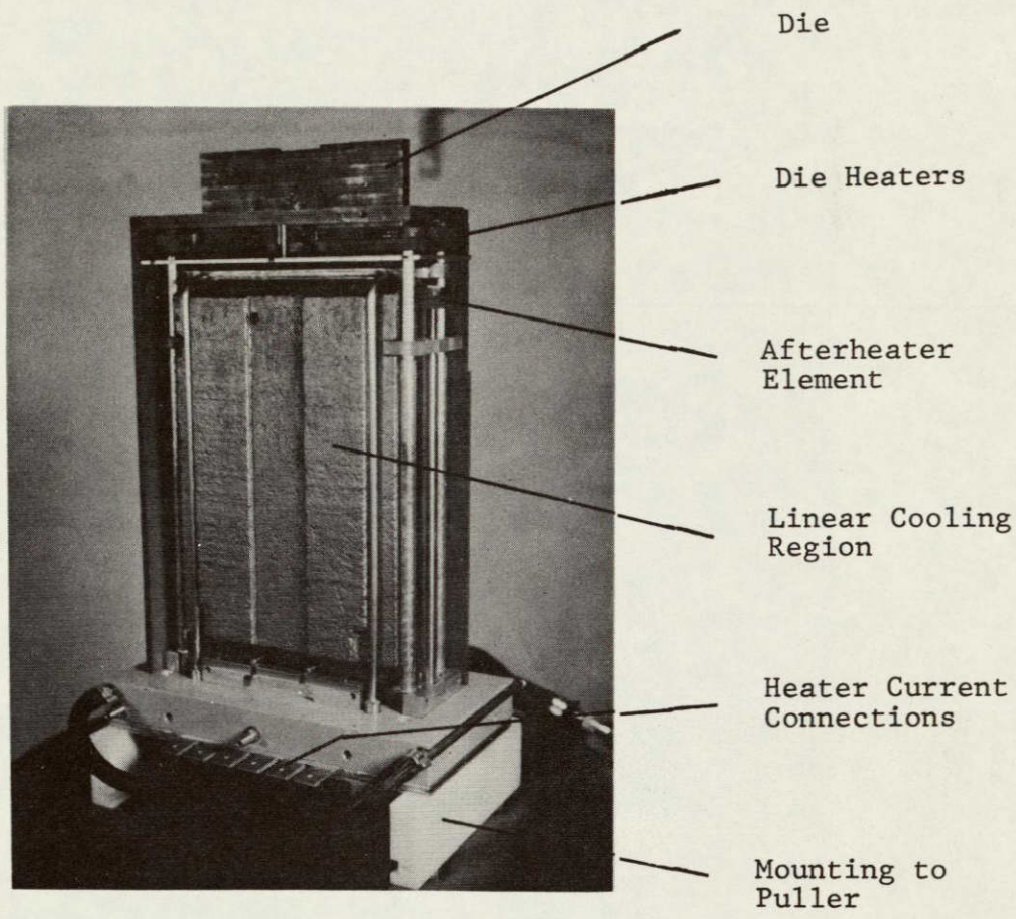

Fig. 3. 10 cm cartridge with side wall and cover removed.

IV. CELL AND MATERIALS CHARACTERIZATION

A. Cell Characterization by C.T. Ho

1. Overview

Towards the end of 1978, MTSEC started to discontinue its standard solar cell fabrication process which is being replaced by an internally developed new "low-cost" process. This process is now in its shakedown phase, and although it has proven to be capable of producing solar cells of the same quality as the old process, its execution is still not completely trouble-free and the yields are therefore sometimes low

Under these circumstances, we find it inadvisable to process ribbons from this contract into solar cells for the purpose of materials evaluation until we are convinced that the current problems in the process are reliably resolved. As a consequence, the emphasis of the photovoltaic evaluation of the grown ribbon has been shifted toward Schottky barrier device. This includes (i) a redesign of the metal barrier configuration for the surface photovoltage (SPV) measurement, and (ii) a development of an alternative method to measure diffusion lengths in ribbon material.

2. New Barrier Configuration for SPV Measurement

The regular bulk diffusion length evaluation for a grown material is obtained on a standard 1.9 x 1.9 cm^2 square area Schottky diode formed by an evaporation of 125 $\mathring{A}$ aluminum on the p-type ribbon. Since the ribbon is characterized by a highly inhomogeneous distribution of recombination states, the large area Schottky diode tends to obscure the effects of the distribution. The measured diffusion length often yields an unrealistic average value for the whole metal coverage area.

To overcome the problem, we have redesigned the barrier metal configuration as shown in Fig. 4. In the new configuration, there is a row

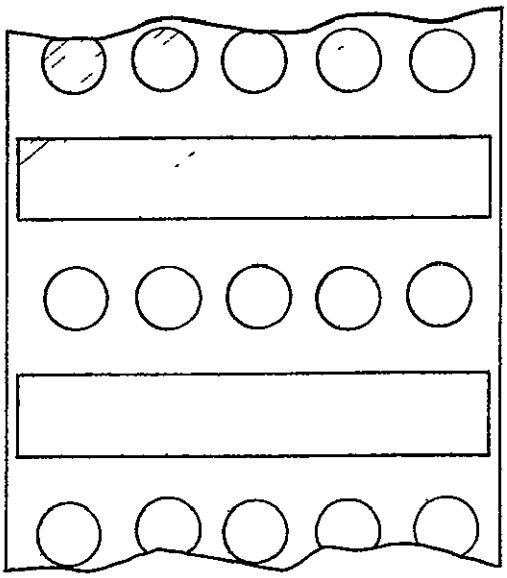

Fig. 4. New Schottky barrier metal configuration for the evaluation of resistance furnace-grown ribbons.

Table III. Comparison of the Diffusion Length Measurement Results from IRPV Method and the Surface Photovoltage Method with Two Data Reduction Techniques.

Cell No.	IRPV	SPV	
		Linear	Nonlinear
18-109-1A	7.9	0.3	9.4
-1B	7.1	2.2	10.4
18-109-5A	10.8	0.3	8.0
-5B	15.4	8.6	16.9
CZ-1	70	81	106
CZ-2	67	80	105

of five 0.95 cm diameter circular diodes and one 5 x 0.95 cm^2 rectangular strip traversing the width of the ribbon. From the circular diodes, we sample the diffusion length value at these five positions, and from the rectangular diode we are able to find out the relative distribution of diffusion length when a long wavelength monochromatic light (e.g., λ = 1.0 μm) is used to scan across the entire width.

Using the above scheme, we re-measured the diffusion length for several ribbons grown from earlier runs, and found better correlation with the solar cell data. In the following material characterization section, the reported SPV diffusion length data were all taken with the newly designed geometrical configuration, but still using linear fit data reduction.

3. IRPV Diffusion Length Measurement on Schottky Device

The employment of surface photovoltage (SPV) measurements on nonuniform and short diffusion length material has been carefully re-assessed. The main reason for concern is that the assumption of the constancy of quantum efficiency with regard to wavelength is no longer valid when the material is inhomogeneous and contains randomly distributed recombination states. We are considering the use of an alternate method, based on our infrared photovoltaic current measurement, to obtain L_n values for bulk ribbon material which might show better correlations with subsequent solar cell results when material is used that is inhomogeneous through the thickness.

The proposed infrared photovoltaic current (IRPV) method on Schottky barrier device involves a simultaneous measurement of reflection, r, and the short circuit current, I_{sc}. A reflectance, r, calibration curve was first established from the measurement of three known reflectance surfaces--one was polished silicon, the other two were aluminum thin films with different thicknesses. Then, the calibration was translated into a photodiode signal through one branch of a bifurcated optical fiber guide. The other branch was used to transmit infrared light at λ = 1.0 μm for the photovoltaic current measurement. The diffusion length, L_n, is obtained from the expression

$$I_{sc} = q\,A\,N_o\,(1 - r - a)\,\frac{\alpha L_n}{1 + \alpha L_n},$$

where a is the absorptance of the evaporated aluminum film, A is the illuminated area, q is the electronic charge, and α is the absorption coefficient at λ = 1.0 μm.

We tested the measurement technique on short diffusion length ribbons taken from run 18-109, as well as on a CZ grown single crystal silicon. The measurement results are shown in Table III. The measured values appear to be reasonable, both for CZ control and ribbon samples. We have also included the results from an SPV measurement with two different data reduction processes — a linear fitting and a nonlinear fitting.[4]

The IRPV method is basically simple and straightforward without any complication from the choice of the data reduction procedures. The main disadvantage is that it depends on the shunt characteristics of the Schottky device. For example, if the diode is badly shunted, the method will no longer be applicable because of the difficulty in estimating the short circuit current. However, for a normal Schottky diode, this method offers an adequate means to estimate low diffusion length material for photovoltaic application. A detailed discussion of this technique will soon be written and published elsewhere.

B. Materials Characterization by J.F. Long

1. Overall Material Quality

The succession of runs in Furnace 3A as well as the various growth experiments in Furnace 1 have resulted in no significant increases in material quality this quarter (Figs. 5(a) and 5(b)). Examination of displaced die material reveals that, in general, diffusion length averages for the "A" (high meniscus) side are somewhat higher than for the "B" side. A notable exception to this observation occurs when SiC particle densities on the "A" surface are high (a condition which seems to be atypical of displaced die growth). Diffusion length values are uniformly depressed in this case. Examination of material grown from dies designed to intentionally redistribute impurities has demonstrated that redistribution does in fact occur.

2. Furnace No. 1

a. Side Channel Die Runs (18-111, -113, -115)

This series of runs utilized a side channel die in order to effect redistribution of impurities via fluid flow. The runs were undoped, boron doped, and aluminum doped, respectively. Resistivity measurements indicate both a type and a resistivity distribution in the undoped samples (Fig. 6). Significant levels of aluminum ($\sim 10^{15}$ atoms/cm^3 were found to exist in the center of the samples by IR absorption. As predicted by theory, no resistivity distribution was observed for the

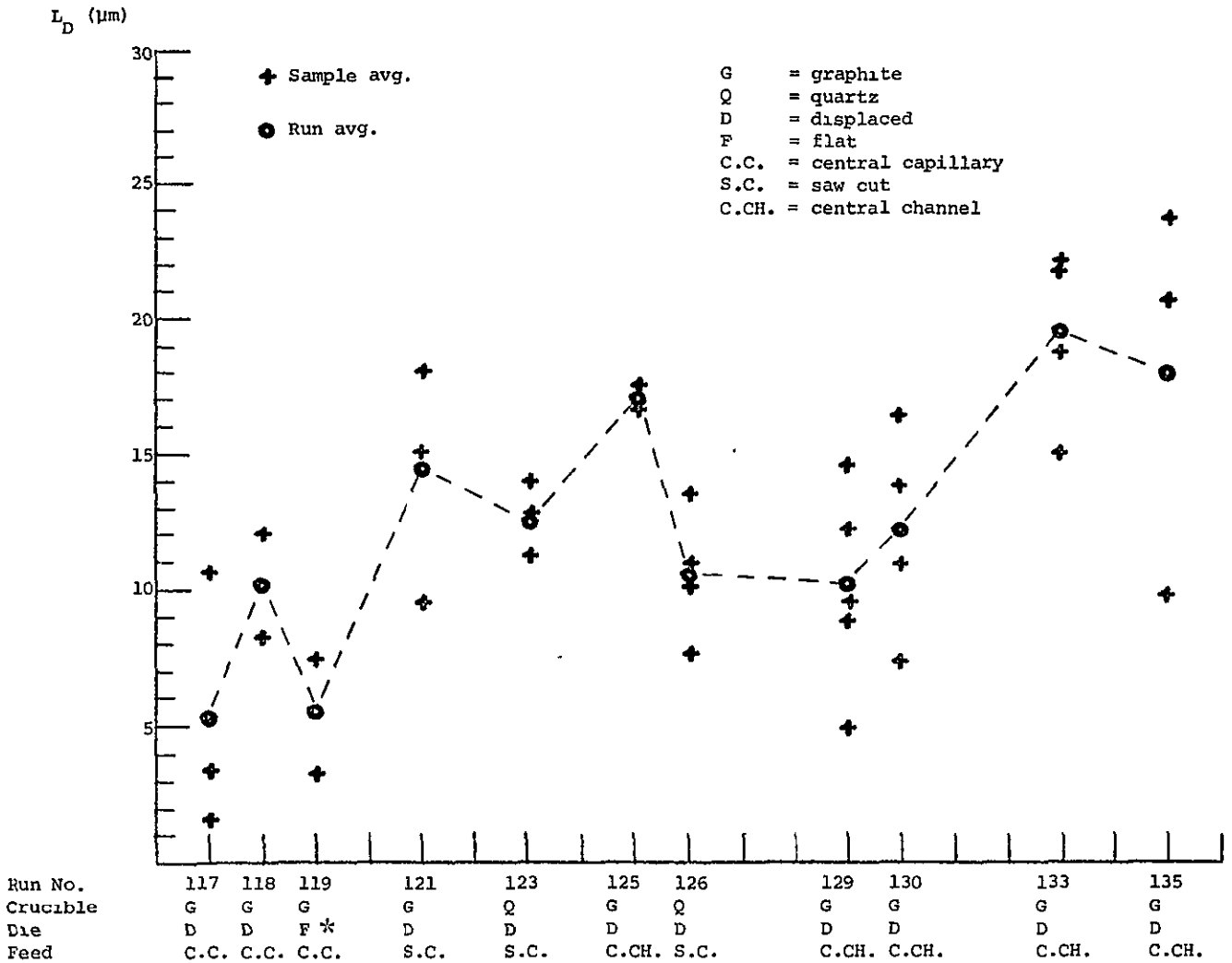

* See footnote on Table 4.

Fig. 5(a). Diffusion length averages for first quarter 1979 (Furnace No. 1).

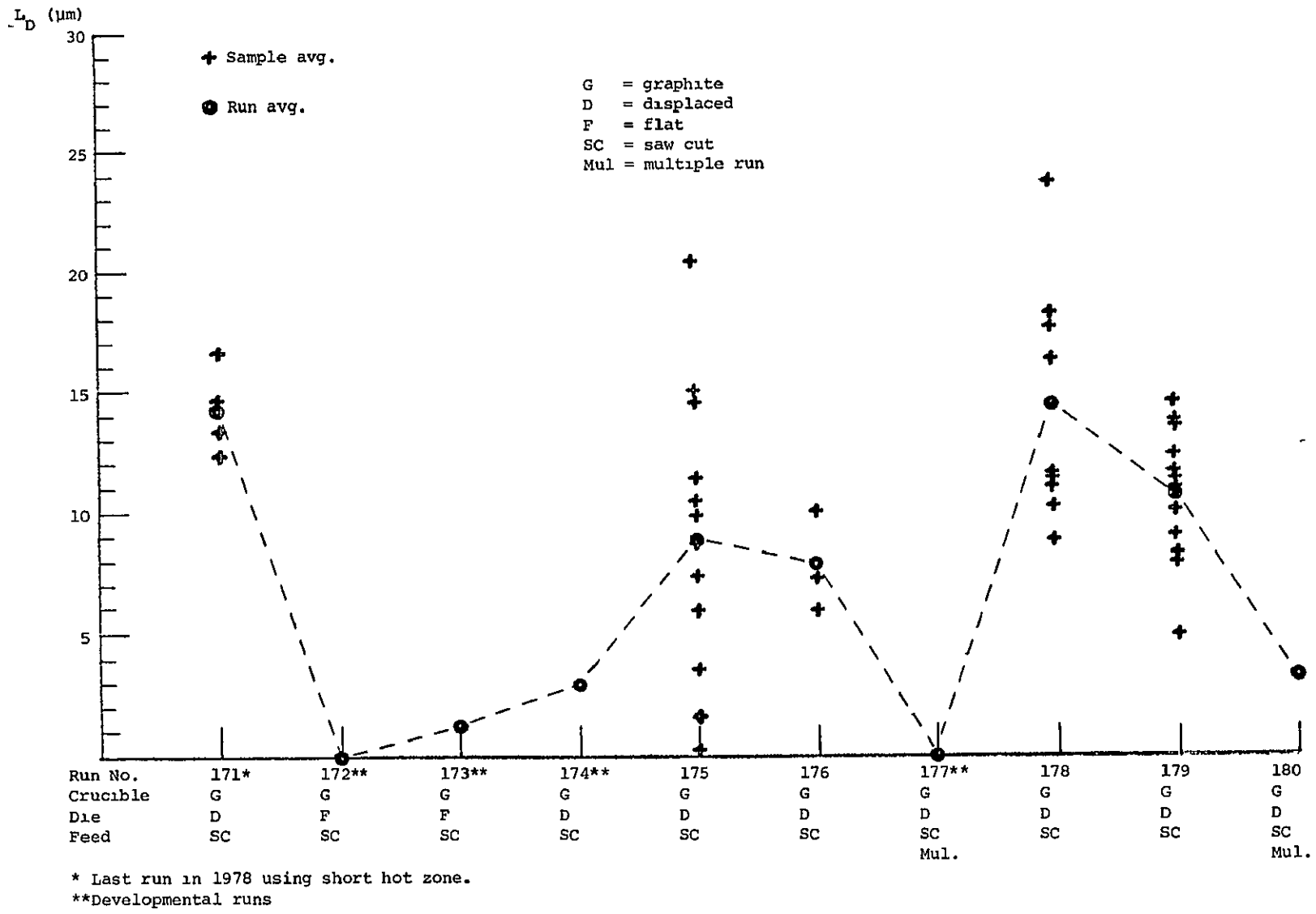

Fig. 5(b). Diffusion length averages for first quarter 1979 (Furnace No. 3A).

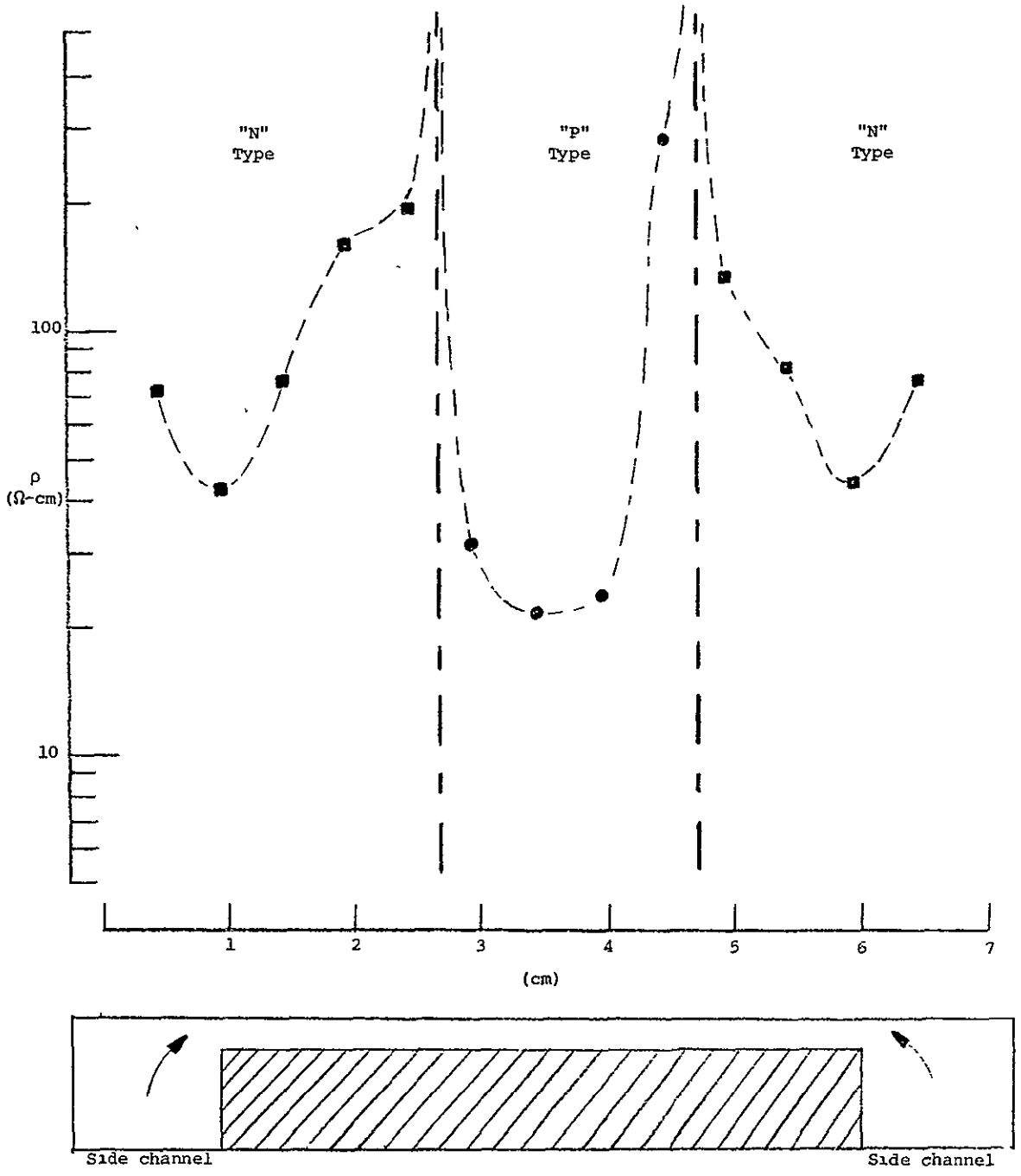

Fig. 6. Resistivity profile for undoped material grown from a side channel die in run 18-111.

boron doped samples. The aluminum doped samples displayed a resistivity distribution indicative of aluminum segregation (Fig. 7).

b. Clean Series of Runs

Routine (Baseline) Runs (18-117, -118, -119): These runs were undertaken to establish a baseline for a graphite insulation system (replacing molybdenum). Diffusion lengths for these runs were found to be somewhat depressed ($\bar{L}_D \leq 10$ μm). The system alterations and subsequent anticipated break-in period may account for this.

Experimental Runs (18-121, -123, -125, -126, -129, -130, -133, -135): These runs were undertaken to investigate the effects of operation with and without a cold shoe. All runs in the series utilized a displaced central channel die. Additionally, within the series of runs which utilized a cold shoe, both graphite and quartz crucibles were used. Finally, two of the runs within the series of runs which omitted the cold shoe utilized a molybdenum insulation package (owing to a graphite insulation system mishap). For all of these runs, no significant differences were observed in minority carrier diffusion lengths as a function of any of the aforementioned growth parameters, although they are consistently slightly lower for the cases of molybdenum insulation and quartz crucible. The data are summarized in Table IV.

3. Furnace No. 3A

a. Developmental Runs (16-172, -173, -174, -177)

Runs 172 through 174 were undertaken to develop melt replenishment mechanism. None of the three was doped, and non-standard operating procedures compromised system cleanliness. Unusually low resistivity values for these runs (0.5 to 13.5 Ω-cm) reflect the degree of contamination. Run 177 was the first multiple growth run of the quarter, and again, non-standard operating procedures resulted in contamination. Diffusion lengths were found to be uniformly depressed. SiC particle densities were found to be atypically high on the "A" surface of this material as well.

b. Clean Runs (16-171, -175, -176, -178, -179)

Run 171 established, in the fourth quarter of 1978, what has thus far been optimum conditions in terms of material quality. It utilized a displaced saw cut die which has become the standard die for

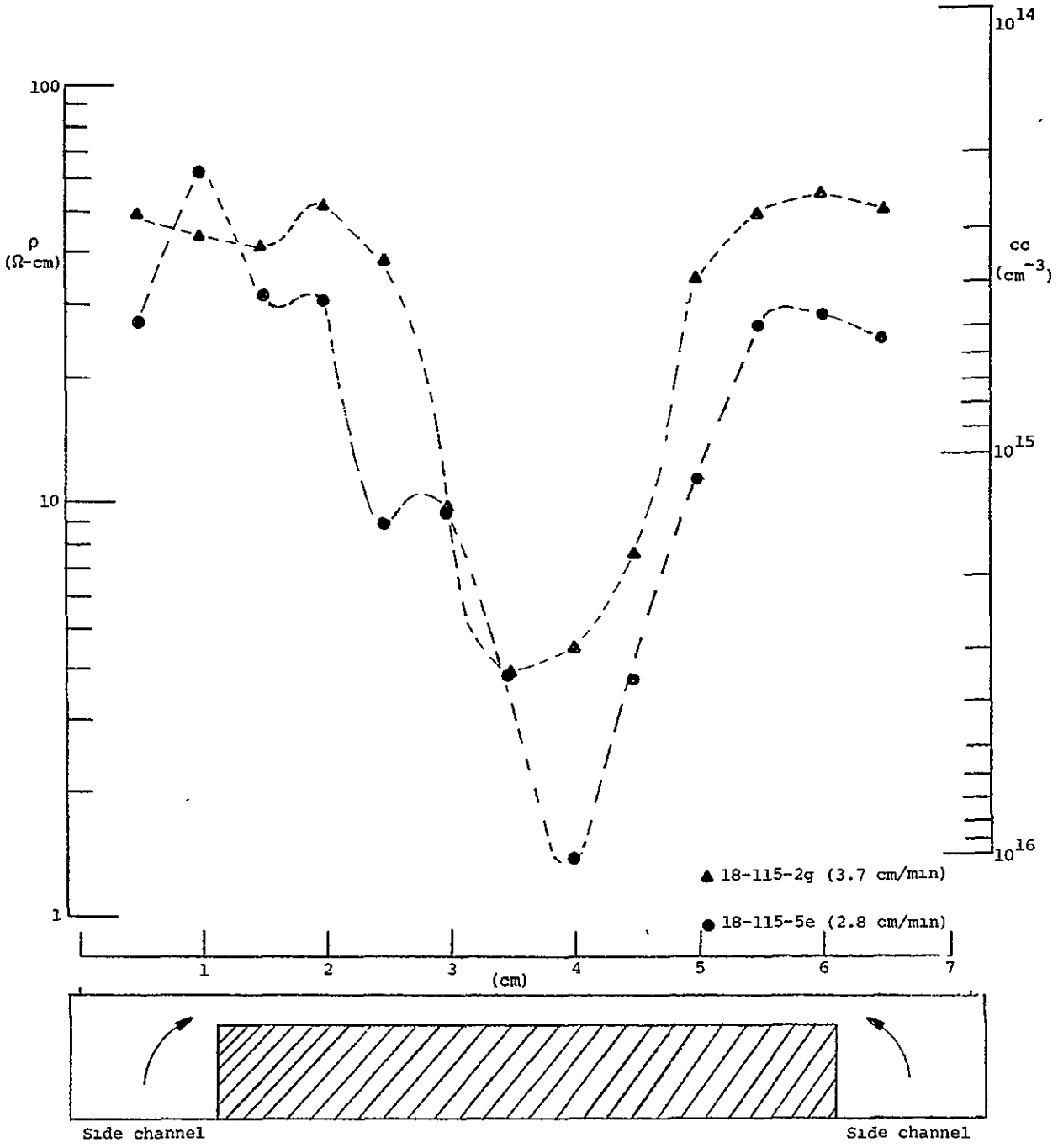

Fig. 7. Resistivity profile for Al doped material grown from a side channel die in run 18-115.

Table IV. Minority Carrier Diffusion Lengths for First Quarter Experimental Series of Runs (Furnace No. 1).

Run No.	Cold Shoe	Crucible	Insulation	$\bar{L}_D$ (μm)
18-117	Yes	Graphite	Graphite	5.3
-118	Yes	Graphite	Graphite	10.1
-119	Yes	Graphite	Graphite	5.4*
-121	Yes	Graphite	Graphite	14.4
-123	Yes	Quartz	Graphite	12.7
-125	Yes	Graphite	Graphite	17.2
-126	Yes	Quartz	Graphite	10.6
-129	No	Graphite	Molybdenum	10.1
-130	No	Graphite	Molybdenum	12.2
-133	No	Graphite	Graphite	19.6
-135	No	Graphite	Graphite	18.3

*This run used a "flat top" die as contrasted with all other recent runs which use displaced dies. Because displaced dies are designed to create lifetime inhomogeneity in the thickness dimension, the numerical diffusion length measurements between displaced die runs and "flat top" die runs may not be comparable.

growth in this furnace. It was the last run prior to the installation of the long hot zone. Minority carrier diffusion length average for this run was 14.0 μm. Runs 175 and 176 were the first clean runs following the testing of the melt replenisher (which was removed for these two runs). "A" surface SiC particles were incorporated in this material, however, and diffusion lengths were found to be lower than optimum ($\bar{L}_D$ < 10 μm). Run 178, following the developmental multiple run, was an attempt to recreate the optimum run conditions without the melt replenisher. This was in fact achieved, with the average diffusion length for the run $\bar{L}_D$ = 14.3 μm. Run 16-179 repeated 16-178, with the melt replenisher in place and operating. The average diffusion length was found to be 13.7 μm. Further, at approximately the midpoint of the run, all cartridge gas flow was terminated. No degradation of diffusion length was observed for material grown after this change (Fig. 8).

c. Clean Multiple Run (16-180)

This run employed five cartridges with melt replenishment. Material from three of the cartridges was examined. "A" surface SiC particle densities were again found to be high, and diffusion lengths were correspondingly depressed. At a point late in the run, all but two cartridges were shut down, and the melt temperature was lowered. SiC particle densities on the "A" surface dropped to near zero, and the diffusion length average ($\bar{L}_D$ = 12.0 μm) rose toward that of the optimum run.

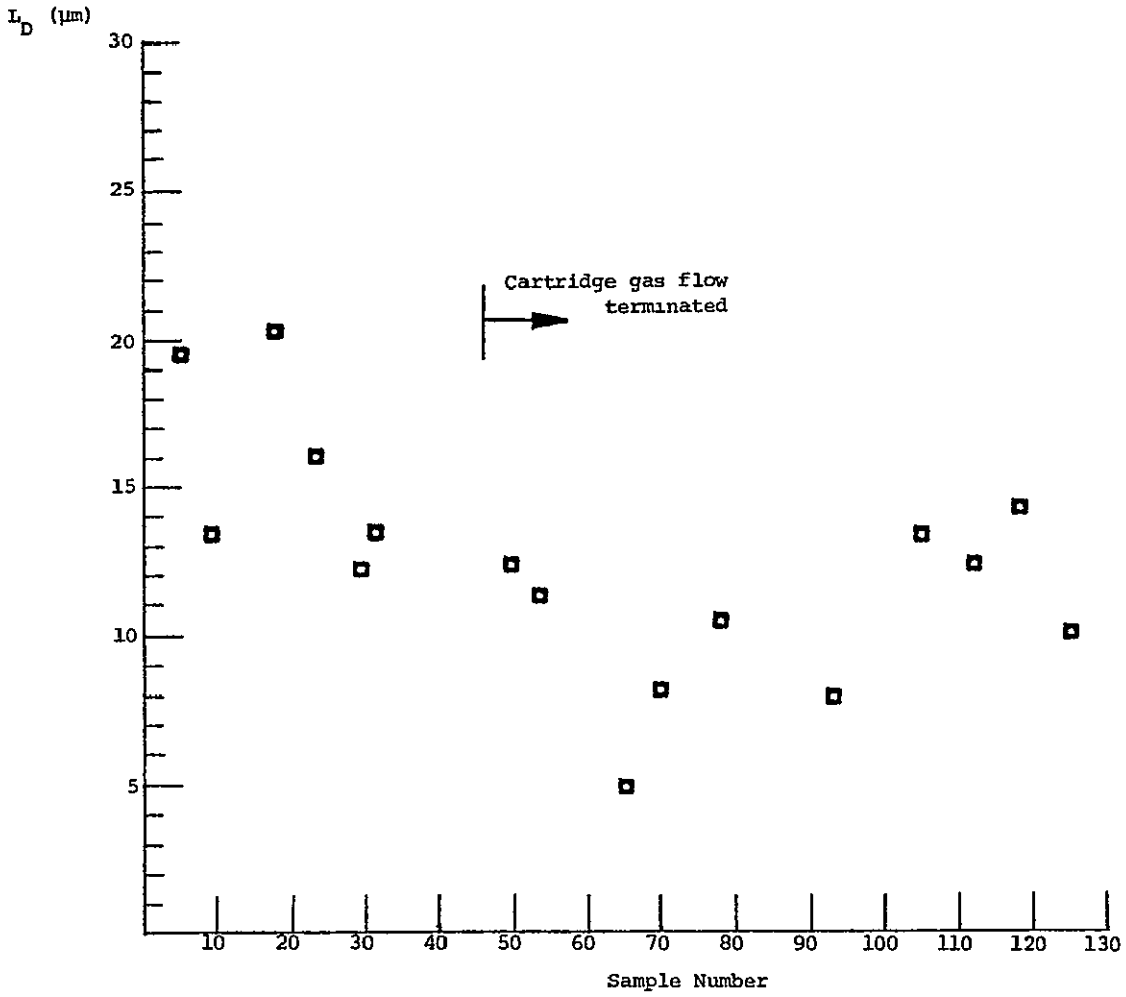

Fig. 8. Sample diffusion length averages for run No. 16-179.

V. MACHINE 17 by E. Sachs

A. Stress Measurement

Stress measurement on grown ribbon is made easier by the realization that in a continuously grown ribbon, the only non-zero stress component is the normal stress along the growth direction. This follows from the arguments presented below.

Since the ribbon is thin, the normal stress perpendicular to the ribbon thickness is negligible. A symmetry argument can be used to show that for axes oriented along and perpendicular to the growth direction, the shear stress is zero. Hence, these are the principal axes. Finally, along any slice made along the growth direction, the resultant of the normal stress perpendicular to the growth direction must be zero. Since, in a continuously grown ribbon, the stress must be the same all along the ribbon length, it must be identically zero.

The techniques examined for the measurement of ribbon stresses include infrared birefringence, in-situ piezo-resistivity, strain gauges, and the multiple cut and split techniques.[3] We have settled on the multiple cut and split technique.

To summarize (see Fig. 9), a ribbon is fastened to a substrate using a low temperature wax along the full length and secured at one end by two glued-on step wedges. The substrate is Kovar, which provides an excellent thermal expansion match to the ribbon, thereby minimizing any stress introduction during the waxing process. The ribbon is then sawn almost its full length in approximately ten even spacings across the width. The substrate is then re-heated, the wax melted, and the strips allowed to relax. The positions of a scribe mark on each ribbon are measured with respect to the edge of the substrate, and these measurements are compared with similar measurements taken before the slicing operation. The resulting displacement of each finger is then used to calculate the stress gradient across the finger width. The complete state of stress may then be

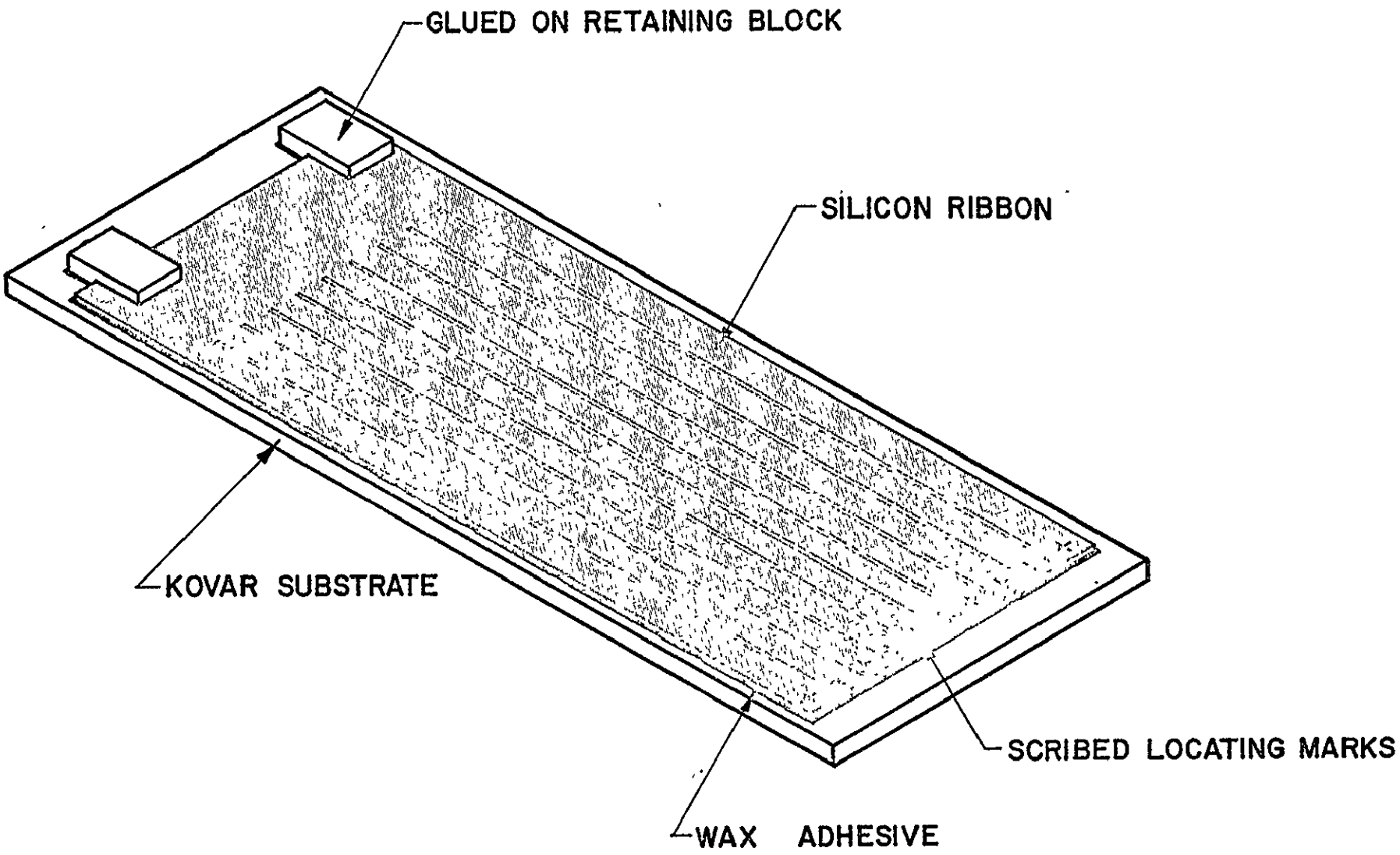

Fig. 9. Multiple cut stress measurement technique.

determined by using the constraint that the net force along any section must be zero since the ribbon is in equilibrium. Equilibrium further demands that the net torque caused by the stress distribution across the width be zero. The magnitude of the moment resulting from the measured stress distribution may thus be used as an indicator of the validity of the measurements.

Data on eight samples taken by this technique is shown in Figs. 10 through 13. The pair of graphs in each figure represents two samples from the same run at the same afterheater setting. Each figure presents data taken at different afterheater settings: 1015°C, 1040°C, 1070°C, and 1130°C. The stress (psi) is plotted against ribbon width (inches), positive stress denoting tension. The ribbon thickness for each of the "fingers" is indicated on the graphs in mils. Also given for each graph is σ_{avg}, the average of the absolute value of the stress across the width. In all cases, the growth speed is 1.9 ± .15 cm/min.

The first thing to note is the consistency between measurements of ribbon grown at a given afterheater setting. Ribbon grown at higher afterheater temperatures does indeed show lower stress levels as may be seen from the stress distributions and the average stress numbers.

Another point of interest is that on several of the graphs (Figs. 11 (a) and 11(b), 12(a) and 12(b) the stress plots exhibit significant local perturbation at fingers which are thin compared to their immediate neighbors. This is perhaps due to increased stress relaxation in thin section.

These plots serve to increase our level of confidence in the multiple cut and split technique of stress measurement. In the next month, we will grow ribbon at similar afterheater settings with an afterheater element which delivers more power to the center. This will serve to shape the horizontal isotherms in a concave downward fashion, and hopefully reduce stress levels.

B. Dynamics

The anamorphic optical-video system and associated video analysis equipment provides a means of obtaining the relevant geometrical information on meniscus heights and ribbon edge positions. The cartridge face and end heaters provide the means for controlling the growth. All that is needed to effect closed loop, optically based control of the growth is the interfacing control hardware which will determine and implement the necessary corrective action to the heater power levels. The design of this control hardware can only proceed on the foundation of a good under-

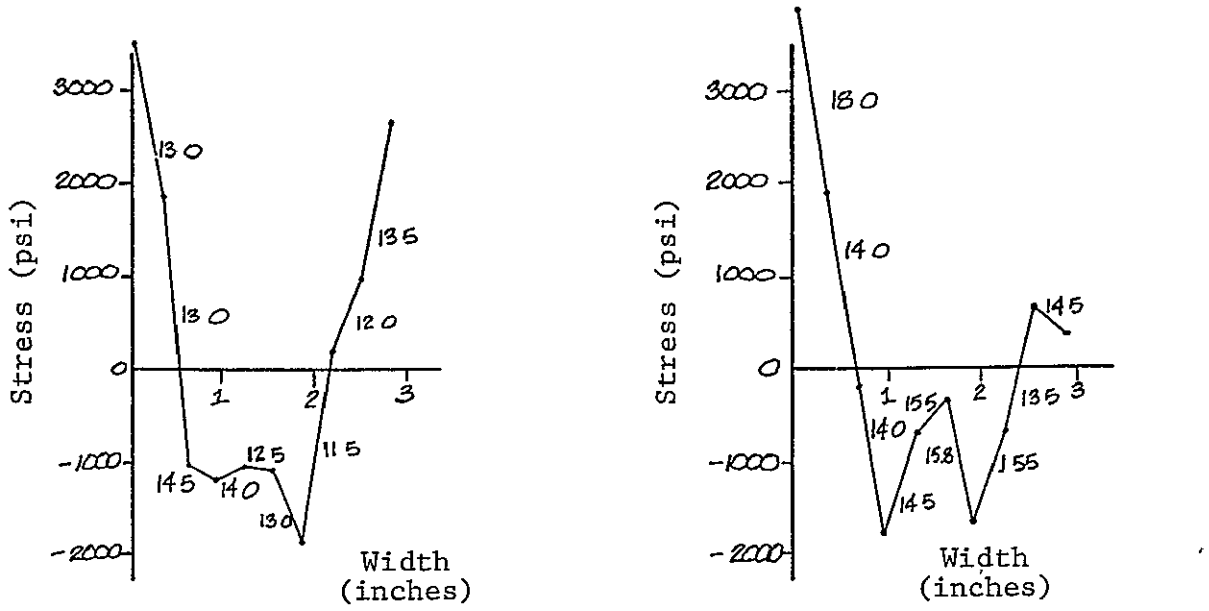

Fig. 10. Ribbon stress measurements - afterheater temperature - 1015°C.

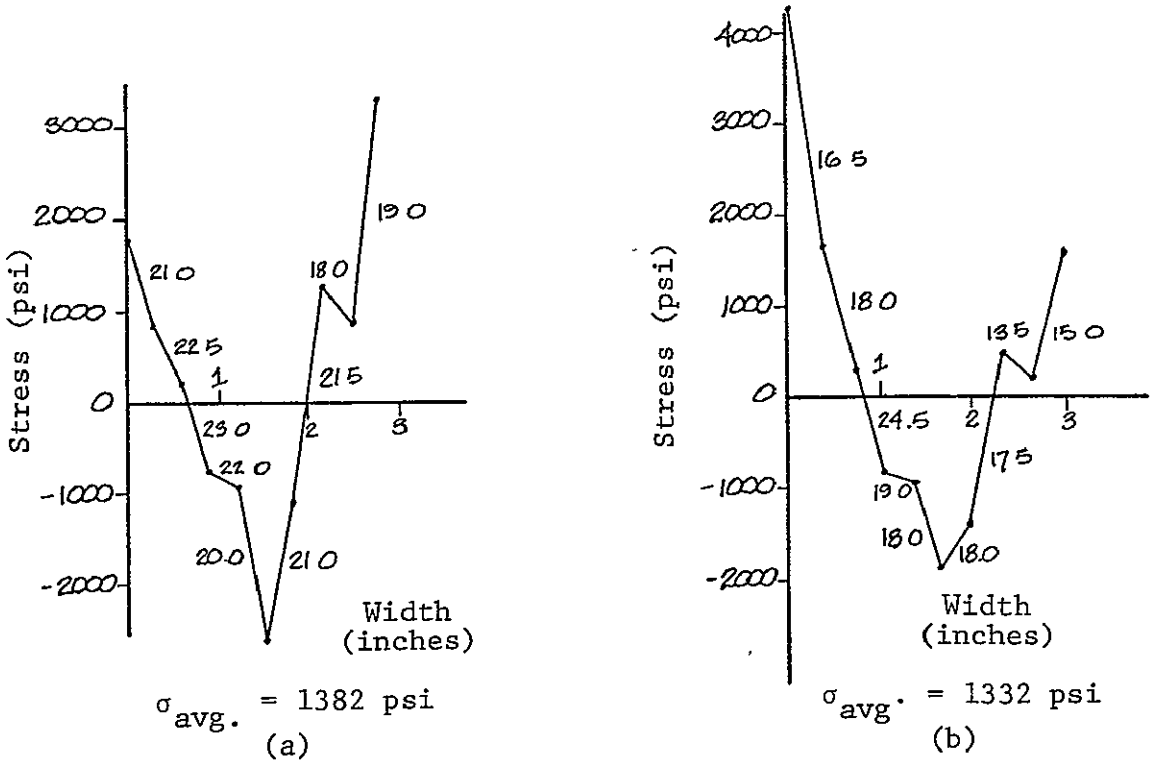

Fig. 11. Ribbon stress measurements - afterheater temperature - 1040°C.

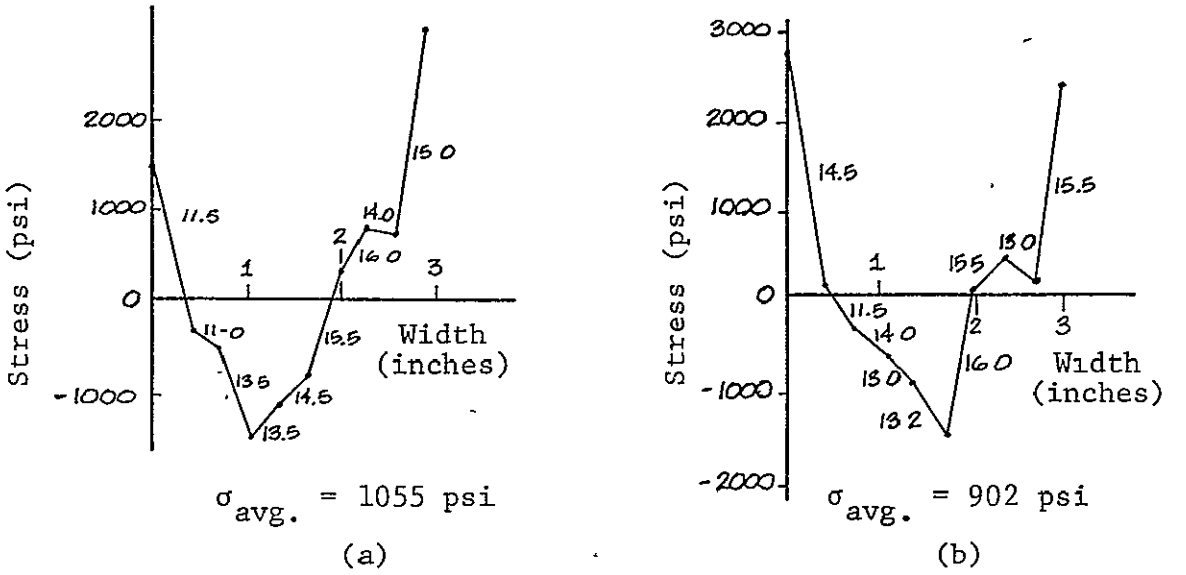

Fig. 12. Ribbon stress measurements - afterheater temperature - 1070°C.

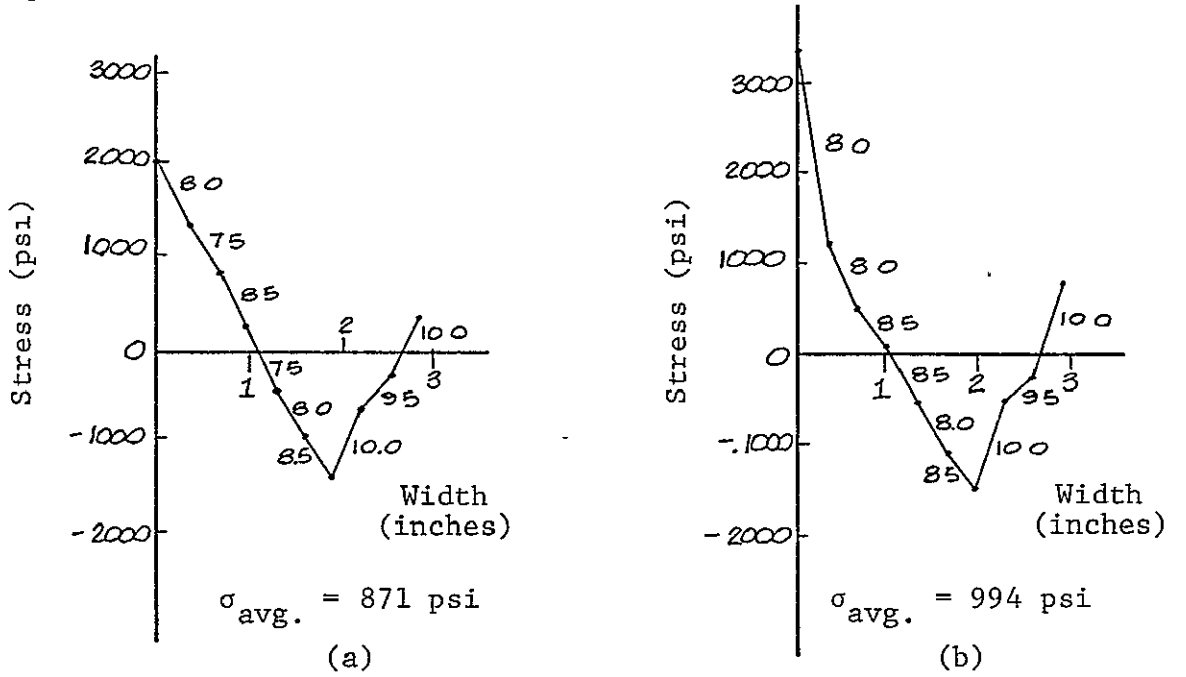

Fig. 13. Ribbon stress measurements - afterheater temperature - 1130°C.

standing of the dynamics of EFG. Such is the primary motivation for these dynamic studies.

The dynamics of the meniscus (as opposed to the edges) is being examined first. These dynamic investigations will follow these lines:

1. Die "tip" temperature response to changes in face heater power level.

2. Meniscus height and ribbon thickness response to changes in face heater power level.

3. Meniscus height and ribbon thickness response to changes in pulling speed.

The method of obtaining this data is illustrated in Figs. 14(a) and 14(b). An oscilloscope was placed in with the instrumentation. Both the input (speed or face heater power) and the output (temperature or meniscus height) are then displayed on the oscilloscope. Thus, we are videotaping a split screened image of the growth and the relevant dynamic information. The oscilloscope permits ready measurement of response amplitudes and phase angles. The digital meters record changes in the input speed on face heater power. A simultaneous voice recording allows the addition of any information needed, such as input signal frequency, etc.

Thus, the video tape provides a method taking accurate data rapidly. It may then be analyzed at leisure later.

In order to measure the die "tip" temperature response to face heater power changes, a carbon-silicon ribbon thermocouple was formed at the die tip. A dummy die with no capillaries was used so that the thermal effect of the melt in the crucible might be substantially unaltered without forming a silicon electrical conduction path to the melt. A ribbon was then melted into the top of a die with a .2 cm deep cross-slot designed to help accept the melted ribbon. The ribbon was then frozen to the die. The die, die holding pins, floors and side walls constitute a completely graphite conduction path out of the furnace. Leads attached to the top of the insulated (SiO_2 coated) ribbon and the graphite side wall then constituted a carbon-silicon ribbon thermocouple.

Square wave (Fig. 14(a) and sinusoidal inputs (Fig. 14(b) of varying frequency were then added into the face heater control signal. The resultant die tip temperature excursions were measured from the video-tape record. The results are summarized in Fig. 15 in the form of frequency response and phase angle curves. In the frequency response curve, the log of the response amplitude,

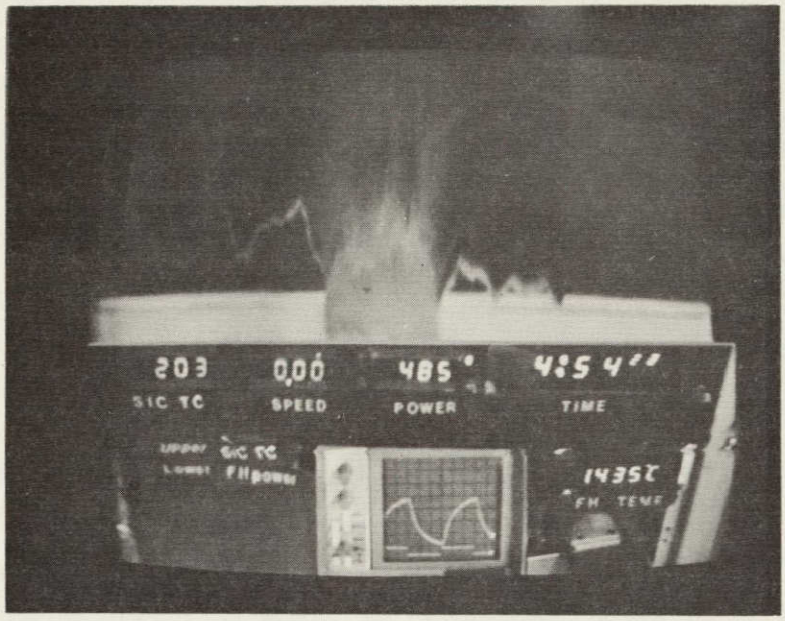

Fig. 14(a). Video tape record of measurement of die tip temperature response to face heater power changes. The top half shows the formation of the carbon-silicon thermocouple between the die and the ribbon. The bottom half shows instrumentation including a storage scope display of power level and thermocouple output. The power level has square wave oscillations added in.

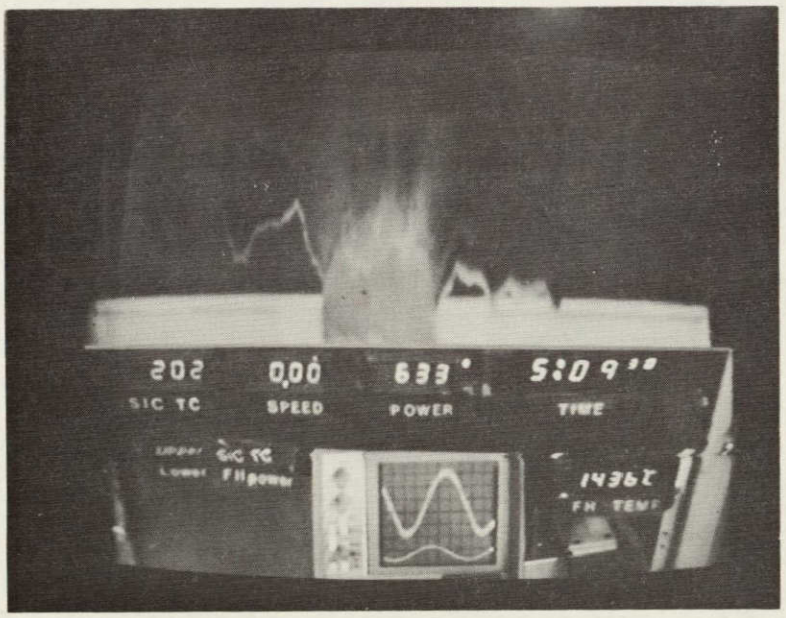

Fig. 14(b). Same as Fig. 14(a), with sinusoidal face heater power oscillations.

$$\left(\frac{|\Delta \text{ temperature}|}{|\Delta \text{ power}|}\right)$$

is plotted against the log of the sinusoidal input frequency. The phase angle plot shows, against the same abscissa, the relative lag angle of the response with respect to the input.

The magnitude and phase response curves are typical of those seen for an overdamped second order system. In the high frequency range, the slope of the response curve is measured to be -49 dB/decade. This compares well with the expected slope of -40 dB/decade for a second order system. (A slope of -40 dB/decade means a factor of 100 increase in input frequency.) The phase angle plot also indicates a second order system as it seems to level out at -180^{o} for higher frequencies. (A first order system would give -90^{o} phase shift; a third order system would give -270^{o}, etc.)

The natural frequency of the system may be found by extending the high frequency response line up to the DC response level, and noting the intersection frequency, resulting in a measured natural frequency of .04 Hz. It should be noted that the phase angle passes through -90^{o} at approximately .05 Hz, just as it should for a second order system.

Finally, a heavily overdamped second order system should be expected to respond to a step change like a first order system, as one of the poles is dominant. Such is, in fact, the case as reference to Fig. 15(a) shows. From the measured response time constant, and natural frequency, a damping ratio may be calculated. It is found to be 3.7. A simple model has been developed for this system, summarized in Fig. 16.

This model consists of two thermal capacitors and three thermal resistors. The heat source (Q) models the joule heat dissipation of the face heater. It may be thought of as the thermal analogue to an electrical current source. The first capacitor, C_1, models the thermal capacitance (thermal inertia) of the heating element itself. The second capacitor, C_2, models the thermal capacitance of the die. R_1 models the heat loss mechanisms from the heating element to the environment, while R_3 models the heat loss mechanisms from the die to the environment, and R_2 models the thermal coupling of heater and die.

A governing second order differential equation may be derived for this model, and expressions may be derived for natural frequency and damping ratio. They are:

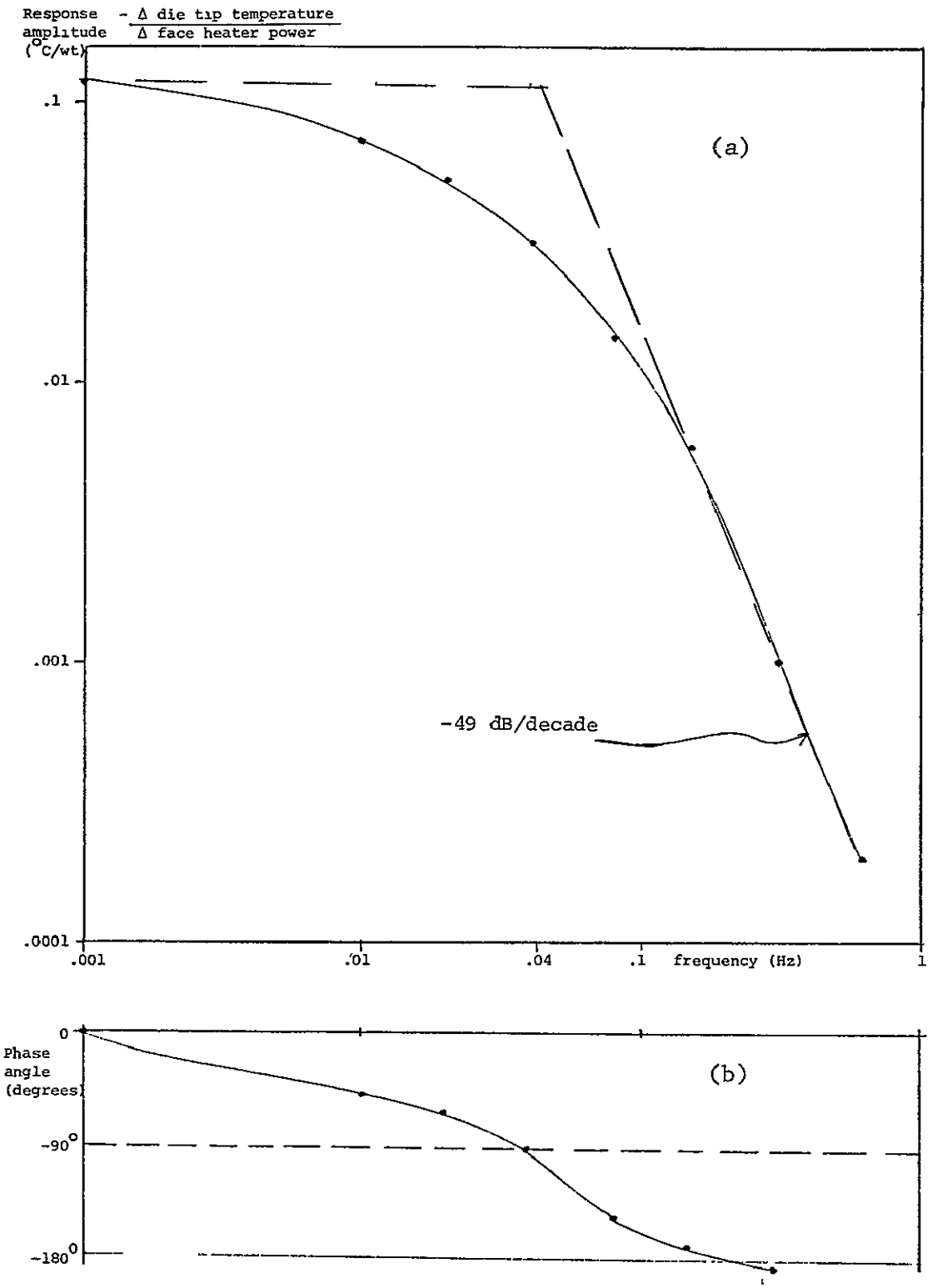

Fig. 15. Response amplitude and phase angle plots as a function of frequency. The face heater power level was varied sinusoidally, and the die tip temperature was observed.

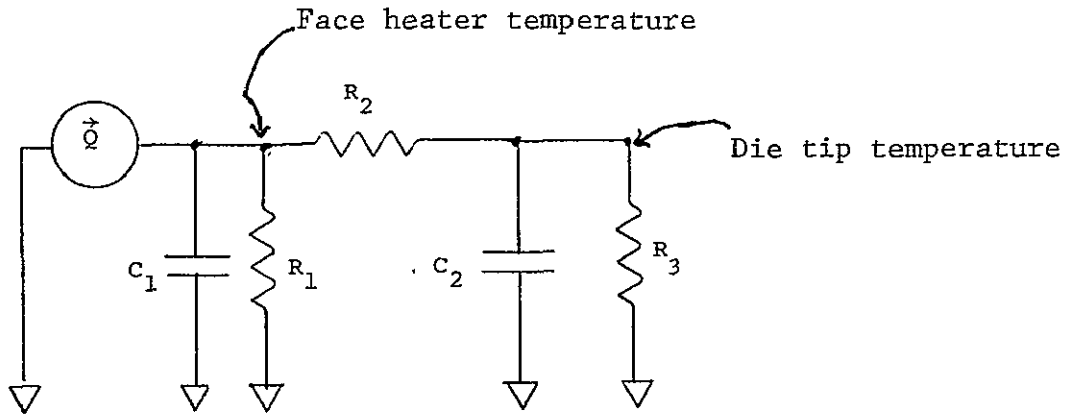

Fig. 16. Lumped parameter model of face heater-die thermal system (see text).

$$\omega_n = \text{nat. freq.} = \left[\frac{R_1 + R_2 + R_3}{R_1\ R_2\ R_3\ C_1\ C_2}\right]^{\frac{1}{2}},$$

$$\text{damping ratio} = \frac{R_1\ R_3\ (C_1 + C_2) + R_2\ (R_1\ C_1 + R_3\ C_2)}{R_1\ R_2\ R_3\ C_1\ C_2\ 2\ \omega_n}.$$

The thermal capacitance s may be calculated to be $C_1 = 2.7$ J/°K, $C_2 = 21.9$ J/°K, where I have used only the mass of the die within the cartridge, as that part of the die below the cartridge floor is largely subject to control by the melt.

R_1 and R_3 may be linearized and computed around typical operating points to be $R_1 \cong R_3 \cong .45$°K/watt. R_2 may be similarly linearized and computed as $R_2 = 1.77$°K/watt. Substitution of these values into the above equations gives

$$\text{nat. freq.} = \omega_n = .056 \text{ Hz},$$
$$\text{damping ratio} = 1.7$$

Thus, the model predicts the natural frequency quite well indeed. It also predicts an overdamped second order system (damping ratio > 1), but not so overdamped as the experiments show. However, overall agreement between the simple physical model presented and the measurements is very reassuring.

The last two of the three dynamic experiments outlined above will be done next month.

VI. REFERENCES

1. F.V. Wald et al., "Large Area Silicon Sheet by EFG," Fourth Quarterly Progress Report, DOE/JPL 954355/78-4 (March 1979).

2. F.V. Wald et al., "Large Area Silicon Sheet by EFG," Annual Progress Report, DOE/JPL 954355/78-3 (February 1979).

3. F.V. Wald et al., "Large Area Silicon Sheet by EFG," Monthly Progress Report (March 15, 1979).

4. R.O. Bell and G.M. Freedman, "Minority Carrier Diffusion Length From Spectral Response Measurements," in: 13th IEEE Photovoltaic Specialists Conference (New York, IEEE; 1978), p. 89.

VII. APPENDICES

1. Updated Program Plan

The program plan shown previously is still in effect.

2. Man Hours and Costs

Previous cumulative man hours were 61,213 and cost plus fixed fee was $2,166,154 through the fourth quarter of 1978. Man hours for the first quarter of 1979 are 6,427 and cost plus fixed fee is $201,032. Therefore, total cumulative man hours and cost plus fixed fee through March, 1979 are 67,640 and $2,367,186, respectively.

3. Engineering Drawings and Sketches Generated During the Reporting Period

Figures 2 and 3.

4. Summary of Characterization Data Generated During the Reporting Period

These data are contained in Section IV.

5. Action Items Required by JPL

None.

6. New Technology

New technology is being separately reported, pending possible patent applications.

7. Other

Preprint, "Aluminum Redistribution in EFG of Silicon Ribbon," by J.P. Kalejs, G.M. Freedman and F.V. Wald, submitted to Journal of Crystal Growth for publication.

APPENDIX 7

Preprint, "Aluminum Redistribution in EFG of Silicon Ribbon," by J.P. Kalejs, G.M. Freedman and F.V. Wald, submitted to Journal of Crystal Growth for publication.

ALUMINUM REDISTRIBUTION IN EFG OF SILICON RIBBON

by

J.P. Kalejs, G.M. Freedman and F.V. Wald
Mobil Tyco Solar Energy Corporation
16 Hickory Drive
Waltham, Massachusetts 02154

ABSTRACT

Impurity transport in EFG of silicon ribbon has been studied with the help of spreading resistance measurements and infrared transmission spectroscopy taken on ribbon grown from aluminum-doped melts. Redistribution of aluminum dopant is observed both in the ribbon thickness and width dimensions. The redistribution pattern across the ribbon width can be explained with the help of a two-dimensional model of impurity transport in the melt ahead of the growth interface. The model predictions have been used to obtain a value for the diffusion coefficient of aluminum in liquid silicon.

1. Introduction

Impurity redistribution by melt convection has been predicted for Edge-defined Film-fed Growth (EFG) of silicon ribbon [1], and concentration distributions for specific impurities in silicon melt have been calculated by numerical solution of the transport equations. [2]. The first experimental evidence for redistribution of one of these impurities (aluminum) is presented here. The model calculations are used to obtain an estimate of the diffusion coefficient for aluminum in liquid silicon.

Impurity redistribution in the width dimension during EFG of ribbon is predicted to arise as a consequence of convection due to melt flow to supply the growth interface in situations where the lateral (i.e., in the width dimension) flow velocity is nonuniform. Concentration levels of segregated impurities in the boundary layer adjust in response to nonuniformity in the component of melt velocity parallel to the plane of the interface, as impurities rejected in regions of high velocity are swept to regions of lower velocity. The degree of redistribution is a function of growth speed, the interface segregation coefficient and the liquid diffusion coefficient of the impurity species. Redistribution in silicon melt is predicted to be the most pronounced for impurities with low segregation coefficients ($k_o \lesssim 10^{-2}$) and large diffusion coefficients ($D \gtrsim 10^{-4}$ cm^2/sec). The extent of the redistribution will be a function of the melt flow pattern, which in turn can be manipulated through die design.

Aluminum was chosen as the dopant with which to investigate redistribution effects during EFG of 7 cm wide ribbon. It is electrically active (p-type) in silicon, and the substitutional aluminum which is responsible for the electrical activity also can be detected by infrared (IR) transmission spectrophotometry. Its liquid diffusion and equilibrium segregation coefficients have been measured [3,4,5]. There is considerable disagreement in the literature over the magnitude

of the former. However, the segregation coefficient (k_o = 0.002 [5]) is low enough such that the degree of redistribution is expected to be a sensitive function of the diffusion coefficient over the range of reported values. For this reason, observation of redistribution provides a means for obtaining an independent measurement of the diffusion coefficient of aluminum in liquid silicon.

2. Experimental Details

The die design chosen for the investigation of aluminum redistribution is shown in fig. 1. The EFG die used consisted of two pieces of graphite, machined to fit together and pinned as shown in fig. 1(a). The function of the die bottom is to assist in bringing the silicon melt to the growth interface. Its design does not enter into the impurity redistribution considerations to be discussed here. The die top is shown in cross section in fig. 1(b). The capillary feed path consists of vertical side channel slots extending approximately 1.25 cm into each edge of the die, and a die top slot of depth 0.25 cm. The capillary dimension perpendicular to the plane of fig. 1 (b) is 0.050 cm. The overall width of the die is 7.6 cm; the widths of the ribbon grown on which data will be reported ranged from 6.8 to 7.2 cm. The die top flats were machined to a thickness of between 0.005 and 0.010 cm.

Silicon ribbon was grown with a high speed cartridge EFG system described elsewhere [6]. The silicon melt was contained in a crucible made from DFP-2* graphite. The die was fabricated from the same material. Both die and crucible were halogen treated at 2000°C in order to reduce levels of contaminating impurities. Growth speeds varied from 2.5 cm/min to 4.0 cm/min, and ribbon thicknesses ranged from 0.025 cm to 0.060 cm.

---

*DFP-2 is manufactured by Poco Graphite, Inc., Decatur, Texas.

Information on the distribution of electrically active impurities in the ribbon has been obtained from spreading resistance measurements and IR transmission spectrophotometry. The latter was capable of detecting substitutional aluminum and boron. Ribbons grown from both the undoped melt and a melt doped to a resistivity of 2.5 Ω-cm with aluminum were examined. The charge material for the undoped run was 500 Ω-cm p-type polycrystalline silicon. A given aluminum dopant level was achieved by adding Czochralski-grown aluminum-doped silicon to this high resistivity charge. The average Czochralski-grown silicon resistivity was 0.7 Ω-cm. Boron was also detected spectroscopically in the latter. An additional possible source of boron in the ribbon was from contamination of the die top during seeding with a ribbon seed containing boron. The levels of impurities, other than aluminum and boron, in the ribbon and charge were not determined.

The IR transmission spectrophotometry employed to detect the aluminum and boron was carried out at 80°K. Sample size was on the order of about 1 cm x 4 cm, with the longer dimension taken along the ribbon growth direction. Care was taken to minimize vignetting of the 1 cm x 2 cm IR beam by the sample and its holder in order to maximize instrumental resolution, and hence sensitivity. Aluminum concentrations were determined by measuring the absorption coefficients of the (1s → 2p2) transition at ~478 cm^{-1}. A simplified expression for the absorption coefficient, α, was applied: $\alpha = (1/X)\ \ell n\ (I_o/I)$. Here, X is the sample thickness, I_o and I are the relative baseline and transmitted beam intensities at peak wavelength, respectively. Aluminum-doped Czochralski silicon standards were used to obtain a calibration for α against the aluminum concentration. Hall-Van der Pauw measurements were also made on the standards to confirm specified impurity concentrations. Boron level determinations and calibrations were obtained by the same procedure. The (1s → 2p4) transition at ~320 cm^{-1} was monitored for this purpose. All impurity concentrations were converted to resistivity values

using the data of Sze and Irvin [7]. The detection limits for aluminum and boron were estimated at ~1 x 10^{15} atoms and ~3 x 10^{14} atoms/cc, respectively, for the thickness range of samples available.

3. Experimental Results

Examples of resistivity variations observed in undoped and doped ribbon, as obtained from two-point probe measurements, are given in figs. 2 to 4. The data in figs. 2 and 3 are taken across the width of ribbon grown from the undoped and doped melts, respectively, perpendicular to the growth direction. The probe spacing was 100 μm. The traces in figs. 2(a) and 3(a) represent data taken on a 5^{o} bevel traversing the ribbon cross section on a line approximately equidistant from the two ribbon surfaces; the traces of figs. 2(b) and 3(b) are obtained from measurements on the as-grown ribbon surface. The capillary geometry near the die top is shown in schematic cross section along with the resistivity traces. Representative data from measurements taken across the ribbon thickness and along the growth direction down the 5^{o} bevel are shown in fig. 4 for locations separated by about 1 cm along the ribbon width. These data are taken on the same sample as those in fig. 3. The probe spacing for the thickness traces was 50 μm.

Relevant information on substitutional aluminum and boron concentration levels obtained by IR transmission spectroscopy is given in table 1. These measurements were made on ribbon samples adjacent to those from which the data of figs. 2 to 4 were obtained. The substitutional aluminum detected in the central 2 cm section of ribbons grown from the undoped as well as the doped melts is sufficient to account for the lower resistivity in this region. Aluminum is not found in concentrations great enough to be detected elsewhere. The correspondence between the locations of the detected aluminum in the case of ribbon grown from the undoped melt and that grown from the aluminum-doped melt indicates that the former has been con-

taminated by aluminum. This similarity will be exploited in the discussion of the data in the context of the model for convective impurity transport which has been proposed for ribbon EFG.

Boron has been detected in a number of the samples of the ribbon grown from the aluminum-doped melt, but not in that grown from the undoped melt. The major part of the residual boron found in the former is presumed to arise from the boron in the Czochralski dopant material. The presence of the boron contamination reduces the utility of the resistivity data for the purposes of studying aluminum redistribution across the ribbon width. Redistribution of the boron itself by convective transport in the melt is predicted to be minor [2]. This is corroborated by the data in table 1, boron redistribution of a magnitude sufficient to account for the resistivity variations across the ribbon width is not observed. In addition, the contribution of the boron to the resistivity in the central low resistivity regions of the ribbon can be neglected (see table 1 and also figs. 2 and 3). However, the spectroscopic data show the levels of boron detected elsewhere in the ribbon can be great enough to contribute significantly to the measured resistivity. As a consequence, it is not possible to correlate levels of aluminum and the resistivity data in regions of the ribbon where aluminum is not detected spectroscopically.

4. Aluminum Redistribution

The resistivity decrease in the central region of the ribbons grown, in evidence in figs. 2 and 3, and spectroscopic confirmation that substitutional aluminum is present there in greater concentrations than elsewhere in the ribbon, demonstrate that significant redistribution of aluminum occurs across the ribbon width. Redistribution also results in resistivity variations across the ribbon thickness, as shown in fig. 4. The data will now be examined to determine the extent to which the redistribution can be accounted for by impurity transport mechanisms which have been proposed for EFG of ribbon.

Predictions of impurity redistribution across the ribbon width have been made on the basis of a two-dimensional model of convective and diffusive transport arising from melt flow to supply the growth interface [2]. The simplification to a two-dimensional treatment is a consequence of the extreme cross-sectional aspect ratio of the ribbon, which has its width much greater than its thickness. In these circumstances, impurity transport in the ribbon width dimension is convection dominated, while across the ribbon thickness it is diffusion limited at the growth speeds under consideration. It has been further argued that diffusion limited transport in the thickness dimension will not appreciably perturb convective transport in the plane of the ribbon width.

4.1. Redistribution Mechanisms

A necessary consequence of the predicted convective redistribution for aluminum for the present die design is enhancement of aluminum concentration levels above those in the bulk melt in the central region of the ribbon, and depletion of levels below those of the bulk melt elsewhere. The traces in fig. 3 show that, for the ribbon grown from the 2.5 Ω-cm aluminum-doped melt, the average resistivity values in the ribbon center fall below the bulk melt level to the order of 1 Ω-cm; furthermore, the resistivity away from the central minimum increases by an order of magnitude and more above the nominal bulk melt value. As noted above, the data in the higher resistivity regions of the ribbon need not reflect aluminum concentration levels because of the possibility of contamination by boron and other undetected impurities. However, the detection threshhold concentration for aluminum set by spectroscopy provides an upper limit to the average levels near the ribbon edges. The fact that average aluminum levels exceed the detection threshhold concentration (corresponding to a resistivity of about 14 Ω-cm) only in the ribbon center provides important confirmation of the nature of the aluminum redistribution taking place across the ribbon width.

The level of aluminum contamination of the bulk melt in the case of the undoped ribbon examined is not known, except through inference from spectroscopic data (see below), and hence interpretation of the resistivity profiles in fig. 2 is not as straightforward as in the case of the intentionally doped ribbon. However, confirmation of the aluminum redistribution that is taking place with the die design used is obtained from the data by a more indirect means. Characterization of the ribbon by hot-probe thermoelectric conductivity testing indicated strong n-type behavior both on the ribbon face and within the cross section over the 2 cm spans closest to both ribbon edges. This contrasted sharply with the p-type conductivity found in the central 2 cm region of the ribbon, which has been identified as due to redistributed excess aluminum by IR spectroscopy. With this information, it follows that the two extremely high resistivity, cusp-like regions, separating the n- and p-type material in fig. 2, arise as a consequence of the cross-over of the tail of the aluminum-dominated p-type conduction region, created through redistribution, into the n-type material region at the ribbon edge.

The three-dimensional picture of the resistivity variation across both the ribbon width and thickness, provided by figs. 3 and 4, allows identification of features which can be attributed to impurity redistribution taking place on a scale of the order of the ribbon thickness. The variation in resistivity across the ribbon thickness is often considerable, as evidenced in the profiles of figs. 4(c) and 4(f). A specific thickness profile shape in a transverse ribbon cross section, or a given distribution of shapes across the ribbon width from sample to sample, is not consistently reproduced. This diversity in profile shape is taken to reflect a lack of reproducibility in local growth conditions, e.g., such as in the local thermal environment, which influence the interface shape of the ribbon across its width. Impurity transport mechanisms in regions of a non-planar interface are expected to be similar to those in operation in Czochralski growth [8].

Another type of irregularity observed frequently in cross-sectional resistivity profiles takes the form of a resistivity spike, for example, as occurs in the right central portion of the trace in fig. 4(f). The appearance of such inhomogeneities is thought to be associated with the presence of subsurface grain structure in the cross section of ribbon grown in high speed cartridge systems; specific impurity redistribution mechanisms have been proposed to account for the grain structure formation in EFG [9]. Resistivity inhomogeneities on the scale of the ribbon thickness are also observed in the profiles taken across the ribbon width. Most prominent of these are the resistivity peak observed in the central portion of the traces in fig. 2 and the deep minima, reaching almost to the levels of the central region resistivity, occurring toward the ribbon edges in fig. 3(a). Smaller amplitude variations, which are often periodic, are also in evidence, particularly in the central low resistivity regions in figs. 3(a) and 3(b). Except for the case of the central resistivity peak in fig. 2, which will be discussed below, mechanisms that could be responsible for these latter resistivity inhomogeneities have not been identified.

Comparison of the cross section and surface traces in each of figs. 2 and 3 shows that dominant features of the redistribution pattern observed on the scale of the ribbon width are preserved across the ribbon thickness in spite of the presence of local inhomogeneities in resistivity of the kind considered in the paragraphs above. This finding has an important consequence in aiding the understanding of impurity transport in the melt in EFG of silicon ribbon: it suggests that the use of a quasi-two-dimensional model of ribbon impurity transport, which attempts to treat transport in the width dimension independently of processes taking place over distances of the order of the thickness, may be valid over a considerable range of growth conditions. This view is incorporated into the discussion in the next section, where the data of figs. 2 and 3 are used to test the predictions of the proposed two-dimensional model for impurity redistribution on a more quantitative level. Implicit in

the present approach is the assumption that the measured resistivity values in the region of the central minimum, where the detected aluminum concentrations are the highest, are representative of aluminum redistribution taking place on the scale of the ribbon width. The perturbative effects of local inhomogeneities in evidence over distances of the scale of the ribbon thickness, as discussed above, are neglected in this approximation. This and other limitations of the present data in providing a test of the model are discussed below.

4.2 Liquid Silicon Diffusion Coefficient for Aluminum

The extent of redistribution across the ribbon width for a low-k_o impurity, such as aluminum, has been predicted to be a sensitive function of the diffusion coefficient of the impurity species in liquid silicon [2]. In the case of aluminum, a range of values of the diffusion coefficient have been reported in the literature. Measurement of aluminum segregation during Czochralski growth in one instance has been used to deduce a value of $5.5 \pm 2.5 \times 10^{-4}$ cm^2/sec [3]. Other experiments, also in a Czochralski system, have yielded very different results in the range from 0.24 to 0.37×10^{-4} cm^2/sec [4]. In principle, EFG of ribbon has potential as an experimental technique which can also provide information on the diffusion process for impurities in the melt. By way of example, the merits of this approach will be examined in a discussion of the model predictions for aluminum redistribution, and its ability to account for the redistribution effects observed across the ribbon width in the resistivity data presented above.

For a fixed die geometry, ribbon growth speed and impurity equilibrium segregation coefficient, the bulk melt concentration and liquid diffusion coefficient of the impurity species remain as parameters to be specified in the redistribution model calculations. The nominal doping of the melt for the aluminum-doped ribbon characterized here was to a resistivity of 2.5 Ω-cm. This level was confirmed in an auxiliary experiment. Narrow (≃1 cm wide) ribbon was grown from directly above

a vertical capillary on one side of the die to obtain uniform ribbon dopant levels. The average aluminum concentration over the full width of this ribbon, obtained from a single IR scan, was 6.1 x 10^{15} atoms/cc (corresponding to a resistivity of about 2.2 Ω-cm). This is within the estimated experimental error of the measurement, ±15%, of the nominal bulk melt doping level. This concentration was used in the calculations of the concentration profiles for aluminum according to the scheme described in reference [2], with the liquid diffusion coefficient remaining as an adjustable parameter. The calculated concentrations have been converted to resistivity values, and the predicted aluminum contributions to resistivity are compared with the experimental data in fig. 5 for a range of diffusion coefficients encompassing the values reported in the literature. A bulk melt contamination level of 1.6 x 10^{15} atoms/cc (corresponding to a resistivity of about 9 Ω-cm) for aluminum was used to calculate the contribution of the aluminum to the resistivity in the case of the undoped ribbon. This level was inferred from the spectroscopic data in table 1 under the assumption that the total aluminum detected in the ribbon (i.e., in the ribbon center) represents a good approximation to the average bulk melt concentration. The predicted resistivity variation for a single value of diffusion coefficient is compared to the experimental data for the undoped ribbon in fig. 6.

The understanding of aluminum transport gained from the model predictions and the spectroscopic data for the doped ribbon are combined to deduce a value for the diffusion coefficient of aluminum in liquid silicon. Figure 5 shows that, in a range of diffusion coefficients from 3 to 10 x 10^{-4} cm^2/sec, the predicted aluminum redistribution can account for the most prominent feature observed in the experimental data — the decrease of the resistivity in the central section of the ribbon. This region has been confirmed to contain aluminum levels sufficient to account for the measured lower resistivity (see table 1). The upper limit for the diffusion coefficient

is inferred from the observation that, as the diffusion coefficient is increased, the calculated resistivity minimum width starts to narrow substantially below that observed in the data. In the other extreme, as the diffusion coefficient is decreased, the calculated profiles eventually cannot be reconciled with the spectroscopic data. As seen from table 1, aluminum is not detected near the ribbon edges down to a level of 1×10^{15} atoms/cc (corresponding to a resistivity of 14 Ω-cm). However, the aluminum concentration near the ribbon edges is predicted to increase with decreasing diffusion coefficient as a consequence of weaker redistribution effects; thus, already for 3×10^{-4} cm^2/sec, the average aluminum levels at the edges should have surpassed the threshhold detection level. These observations have led to the assignment of a value for the diffusion coefficient of aluminum in liquid silicon of $6.5 \pm 3.5 \times 10^{-4}$ cm^2/sec. This result supports the value quoted above from reference [3]. At the same time, the predicted redistribution for the range of diffusion coefficients reported in reference [4] is very weak (see fig. 5) and in direct conflict with the spectroscopic data for the reasons given above.

5. Discussion

The model results have been shown to be capable of accounting for the most prominent variations in the ribbon width resistivity profiles. Factors contributing to experimental uncertainties in the measurements will now be examined in order to focus on areas in which the data are deficient in providing a test of the redistribution model.

Resistivity variations of the type shown in fig. 4 indicate significant redistribution occurs on a local scale through impurity transport not accounted for in the model. The result is that often the resistivity value obtained at a given width location differs significantly from trace to trace (compare, for example, figs. 3(a) and 3(b)). The large variations which are observed are emphasized in the thickness traces (e.g., fig. 4(c)). Interface shape deviations from an ideal planar profile,

which are held responsible for much of this local inhomogeneity, can be expected to arise from ribbon thickness nonuniformity, departures from ideal melt flow conditions, and the nature of the temperature distribution imposed at the growth interface through system design. Asymmetry in resistivity profiles with respect to the ribbon center line, such as is evident in fig. 3, is attributed to the combined influence of the first two of these factors. An important aspect of the design of the EFG system used here is the large temperature gradient (up to 2000^{o}C/cm) imposed at the growth interface to assist in achieving high growth rates. This subjects the ribbon to large thermal stresses, with the attendant possibility of increases in defect density, hence material inhomogeneity. The temperature field responsible for the high heat removal rates required is also one of several factors influential in determining interface shape. A final consideration in system performance is EFG die design. Die top geometry is expected to have a major influence on interface shape. At present, knowledge of the manner in which system component design affects interface shape and how it may be used to aid in reducing material inhomogeneity is lacking for EFG of silicon ribbon.

Spectroscopic measurements have helped to establish that aluminum is transported to the ribbon center in accordance with the predictions of the transport model. The calculated concentration levels in this central region, but not the shape of the profile, are affected by the experimental error in the spectroscopic data only through the uncertainty in the determination of the bulk melt concentration. It is, therefore, argued that the disagreement between the calculated and experimental resistivity profiles found in the center of the ribbon (see figs. 5 and 6) is significant, both for the doped and the undoped material. The situation is further complicated by the presence of an additional feature in the undoped ribbon profiles, a pronounced resistivity peak superimposed on the central minimum (see also fig. 2).

Possible causes that can be advanced to explain these features differ in the two cases. In the doped ribbon, the predicted resistivity values at the minimum reach lows in the range from 0.3 to 0.4 Ω-cm. The corresponding concentration range, 6 to 8 x 10^{16} atoms/cc, is not far removed from equalling the solubility limit for aluminum in silicon, which is given as 3 to 4 x 10^{17} atoms/cc [5] at the melting point. One possibility raised in view of the predicted low resistivity values is that the level of electrically active aluminum in this region is reduced by the formation of electrically neutral precipitates. Alternately, the high concentrations of aluminum may be responsible for interface breakdown. Additional material characterization is in progress to attempt to resolve these issues.

The predicted maximum aluminum concentration in the undoped ribbon is 2 x 10^{16} atoms/cc, a level at which the above mechanisms are less likely to be activated. If they are accepted as operative, an additional, associated process responsible for the appearance of a resistivity maximum, which is nevertheless absent in the more highly-doped ribbon, now must be postulated for the undoped ribbon. An alternative, more probable explanation to consider is that the resistivity maximum is a compensated region formed by the presence of an undetected n-type impurity redistributed by the same convective melt flow as the aluminum. The concentration of any such redistributed impurity is predicted to be enhanced precisely at the position of the central aluminum resistivity maximum because of its location on the line of symmetry of the velocity field [2]. In the same way, the presence of undetected redistributed n-type impurities in the doped ribbon offers an alternative explanation for the appearance of higher resistivity values in the ribbon center than predicted solely on the basis of aluminum redistribution.

Convective transport arising from melt flow to the growth interface is the only form of convection treated in the model of

impurity transport for ribbon EFG employed here. Other convective transport mechanisms which have been considered for EFG are surface tension-driven flow and thermal convection [2]. No evidence to link unexplained features in the data, such as the resistivity inhomogeneities discussed above, to the presence of such additional modes of convective transport has been found.

6. Conclusions

Impurity transport in EFG of silicon ribbon has been studied through analysis of material grown from aluminum-doped melts. Redistribution of a specific impurity (aluminum) in the melt ahead of the growth interface has been identified for the first time. The redistribution pattern for aluminum across the ribbon width can be accounted for by a two-dimensional model of impurity transport, which treats melt transport in the plane of the ribbon width independently of that occurring in the ribbon thickness dimension. The predictions of the model have been used to deduce a value of $6.5 \pm 3.5 \times 10^{-4}$ cm^2/sec for the diffusion coefficient of aluminum in liquid silicon. This result resolves the disagreement between two independent measurements of the diffusion coefficient in Czochralski growth experiments.

Experimental uncertainty in the data associated with the design of the high speed EFG system used to grow the ribbon for the present study have prevented a full test of the two-dimensional model proposed for impurity transport in the plane of the ribbon width. One source for this uncertainty is inhomogeneity in electrical properties, which has been associated with interface shape variations arising from a non-ideal growth interface environment. Even though aluminum redistribution on the scale of the ribbon width is preserved in the presence of local inhomogeneities, their cumulative effect on the magnitude of the redistribution remains unknown. The possibility of contaminating impurities contributing to the measured resistivity in regions where aluminum concentrations fall below the

threshhold for spectroscopic detection has further complicated interpretation of the data. Nevertheless, the understanding of impurity transport gained in the present investigation shows that EFG has potential as a technique for studying transport processes in melt growth.

Acknowledgements

We wish to thank Mr. C. Radics, Jet Propulsion Laboratory, California Institute of Technology, for carrying out the spreading resistance measurements reported here, and Ms. M.C. Cretella and Mr. J. Long for helpful discussions. This work was performed in part for the Jet Propulsion Laboratory, California Institute of Technology, under Subcontract No. 954355.

References

[1] B. Chalmers, A.I. Mlavsky, T. Surek, J.C. Swartz, R.O. Bell, D.N. Jewett, D.A. Yates, K.V. Ravi and F. Wald, Mobil Tyco Solar Energy Corp., Final Technical Report, NSF/RANN/SE/GI-37067X/FR/75/1, August 1975.

[2] J.P. Kalejs, J. Crystal Growth 44 (1978) 329.

[3] H. Kodera, Japan J. Appl. Phys. 2 (1963) 212. The diffusion coefficient value reported has been adjusted to reflect a different viscosity for liquid silicon, 0.88 cp, used in the numerical calculations presented here.

[4] B.M. Turovskii, Russ. J. Phys. Chem. 36 (1962) 983. The diffusion coefficient values reported have been adjusted to reflect a different viscosity for liquid silicon, 0.88 cp, used in the numerical calculations presented here.

[5] F.A. Trumbore, Bell System Tech. J. 39 (1960) 205.

[6] J.P. Kalejs, B.H. Mackintosh and T. Surek, submitted for publication in J. Crystal Growth.

[7] S.M. Sze and J.C. Irvin, Solid State Electronics 11 (1968) 599.

[8] A. Murgai, E.C. Gatos and A.F. Witt, in: Semiconductor Silicon, 1977, Ed. by H.R. Huff and E. Sirtl (The Electrochemical Soc., Princeton, 1977), p. 72.

[9] C.V.H.N. Rao, M.C. Cretella, F.V. Wald and K.V. Ravi, to be published in J. Crystal Growth.

Table I. Concentrations of Spectroscopically Detected Aluminum and Boron as a Function of Locations Across the Ribbon Width. All Concentrations are Given in Units of 10^{15} atoms/cc. N.D. = Not Detected. The Detection Limits were ~1 x 10^{15} atoms/cc for Aluminum and ~3 x 10^{14} atoms/cc for Boron.

Edge — Center — Edge

(I)	(II)	(III)	(IV)	(V)	(VI)	(VII)
← 1.17 cm →	← 0.7 cm →	← 1.15 cm →	← 1.17 cm →	← 1.17 cm →	← 0.7 cm →	← 1.13 cm →

Location / Ribbon	(I)		(II)		(III)		(IV)		(V)		(VI)		(VII)	
	Al	B	Al	B	Al	B	Al	B	Al	B	Al	B	Al	B
Undoped	N.D.	N.D.	N.D.	N.D.	N.D.	N.D.	1.57	N.D.	N.D.	N.D.	N.D.	N.D.	N.D.	N.D.
Doped	N.D.	0.37	N.D.	N.D.	0.55	0.34	12.0	0.56	0.56	N.D.	N.D.	N.D.	N.D.	N.D.

Figure Captions

Fig. 1. (a) Schematic of two-piece side channel die; (b) cross section view of die top showing capillary channel.

Fig. 2. Spreading resistance (resistivity) profiles taken across the width and perpendicular to the growth direction of a ribbon grown from an undoped melt. (a) trace within ribbon cross section on a 5^{o} bevel approximately midway between ribbon surfaces; (b) trace on the as-grown ribbon surface. The n- and p-type region designations refer to thermoelectric probe identification of net conductivity. Ribbon growth speed was 3.4 cm/min.

Fig. 3. Spreading resistance (resistivity) profiles taken across the width and perpendicular to the growth direction of a ribbon grown from an aluminum-doped melt: (a) trace within ribbon cross section on a 5^{o} bevel approximately midway between ribbon surfaces; (b) trace on as-grown ribbon surface. Ribbon growth speed was 3.7 cm/min.

Fig. 4. Spreading resistance (resistivity) profiles taken across the ribbon thickness and along the growth direction on a 5^{o} bevel for the sample of fig. 3. The traces (a) to (f) are taken at 1 cm intervals across the ribbon width starting about 1 cm from the left-hand edge of the traces shown in fig. 3.

Fig. 5. Comparison of calculated contribution of aluminum to resistivity and doped ribbon data of fig. 3(b) for several values of the diffusion coefficient: (1) 0.24 to 0.37 x 10^{-4} cm^2/sec; (2) 3 x 10^{-4} cm^2/sec; (3) 10 x 10^{-4} cm^2/sec. Dashed line represents bulk melt resistivity level.

Fig. 6. Comparison of calculated contribution of aluminum to resistivity and undoped ribbon data of fig. 2(b) for a diffusion coefficient of 7 x 10^{-4} cm^2/sec. Dashed line represents estimated bulk melt resistivity level.

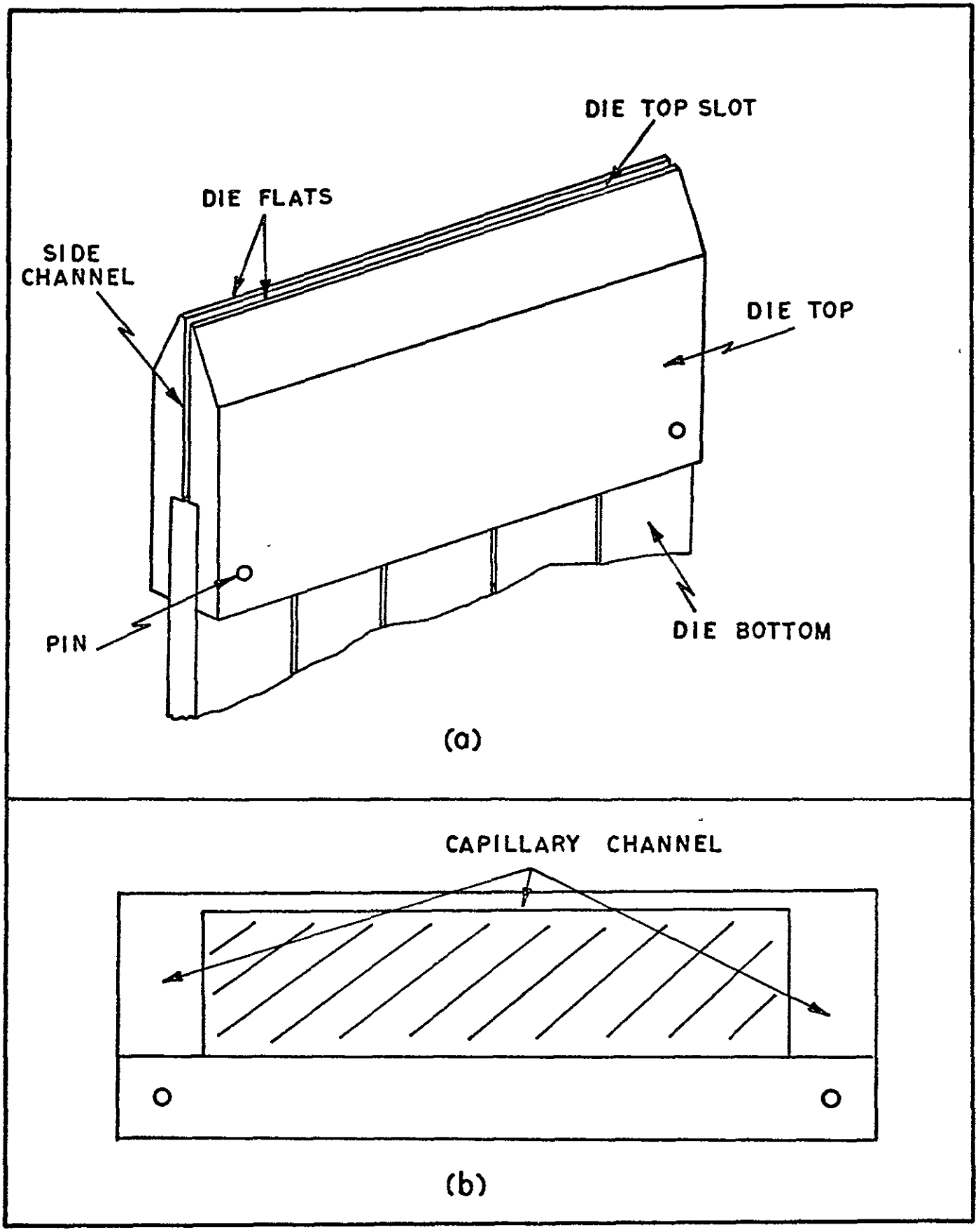
DIE TOP SLOT
DIE FLATS
SIDE CHANNEL
DIE TOP
PIN
DIE BOTTOM
(a)
CAPILLARY CHANNEL
(b)

Fig. 1

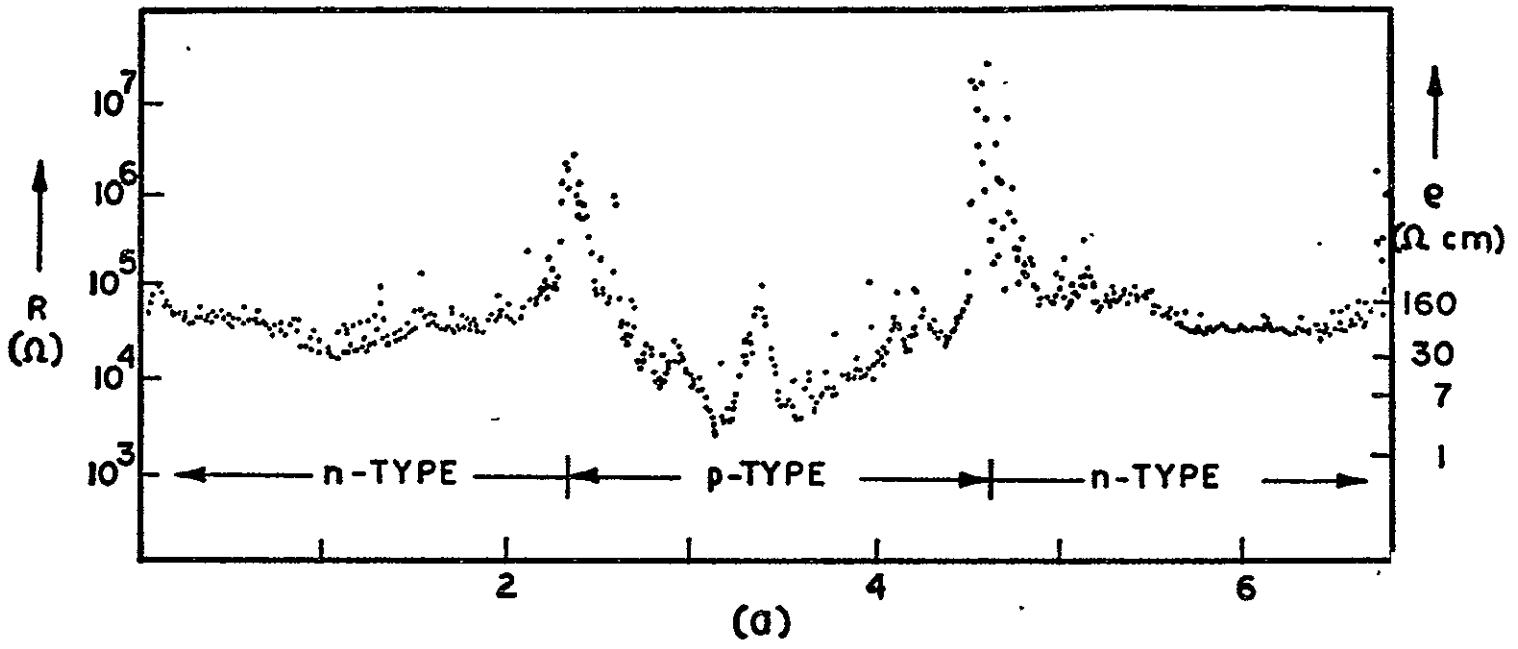

(a)

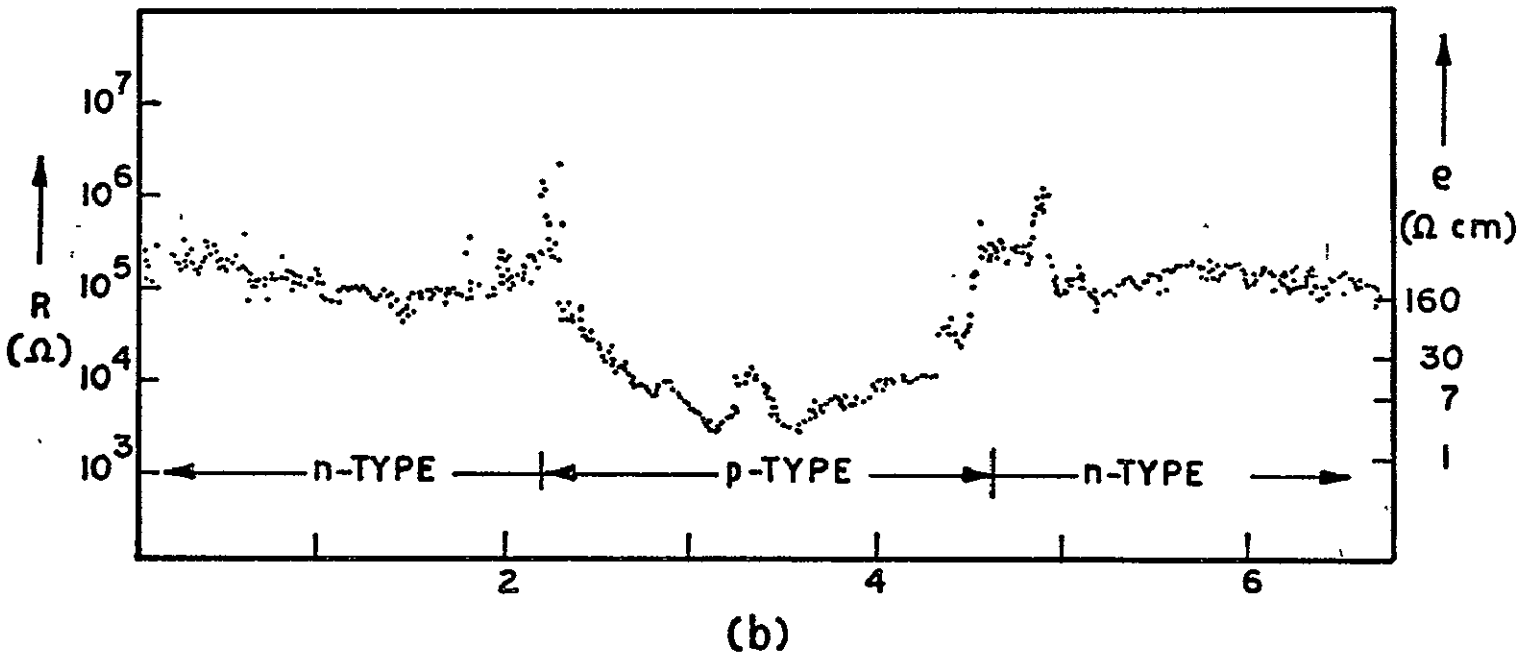

(b)

DISTANCE ACROSS RIBBON WIDTH (cm) ⟶

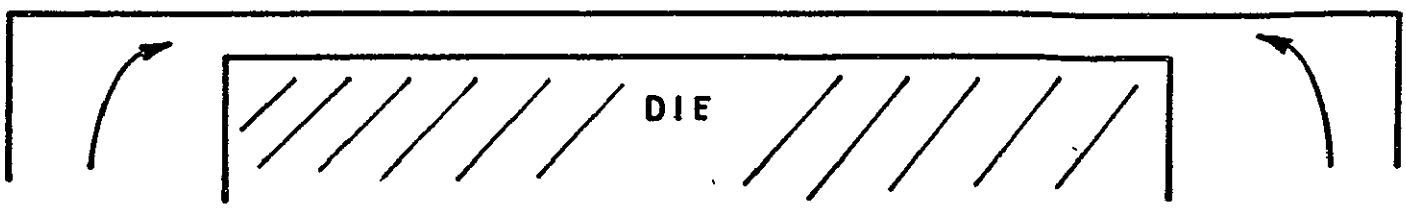

Fig. 2

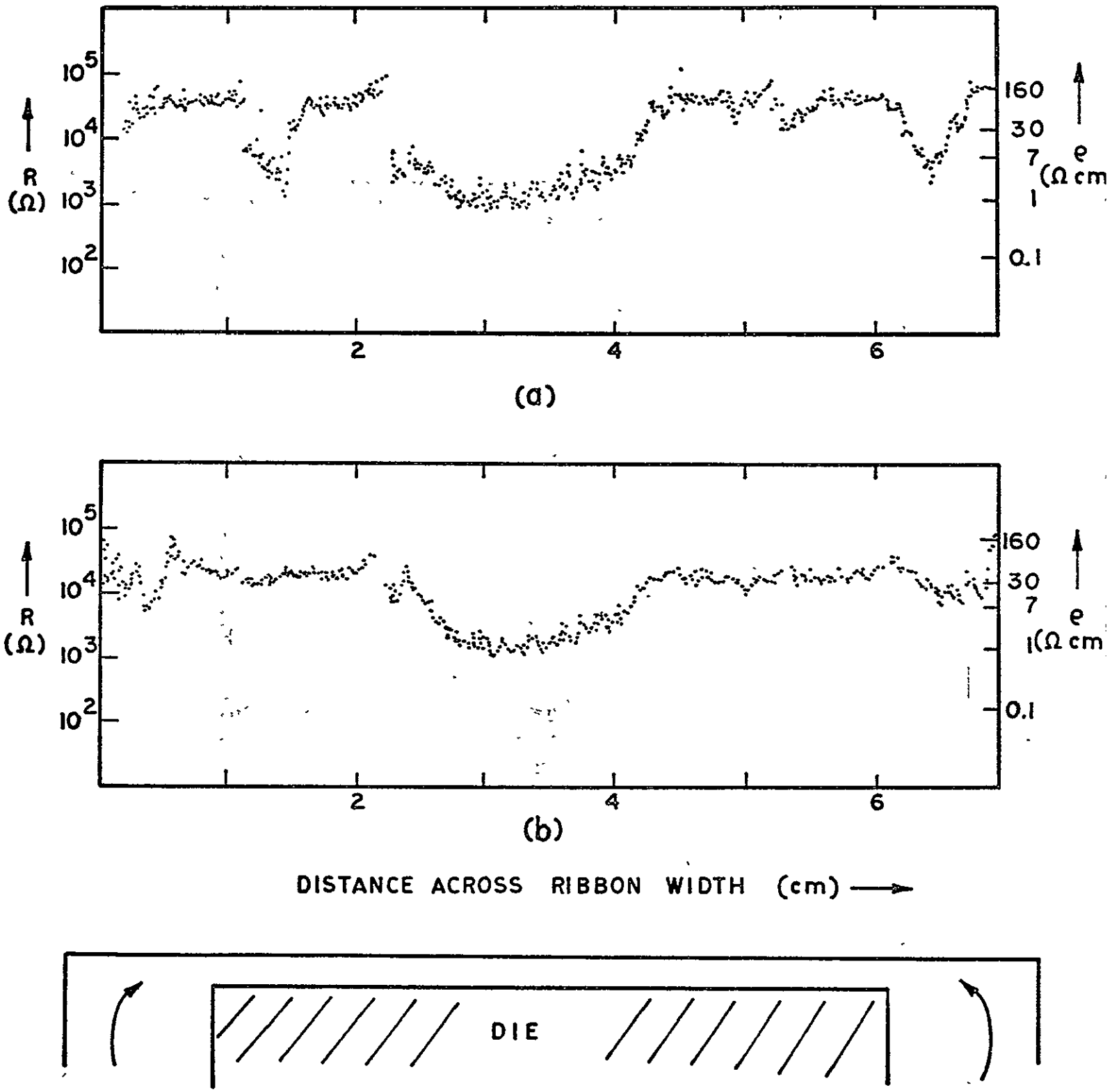
R (Ω)
10^5
10^4
10^3
10^2
160
30
7
1
0.1
e (Ω cm)
2
4
6
(a)
(b)
DISTANCE ACROSS RIBBON WIDTH (cm) ⟶
DIE

Fig. 3

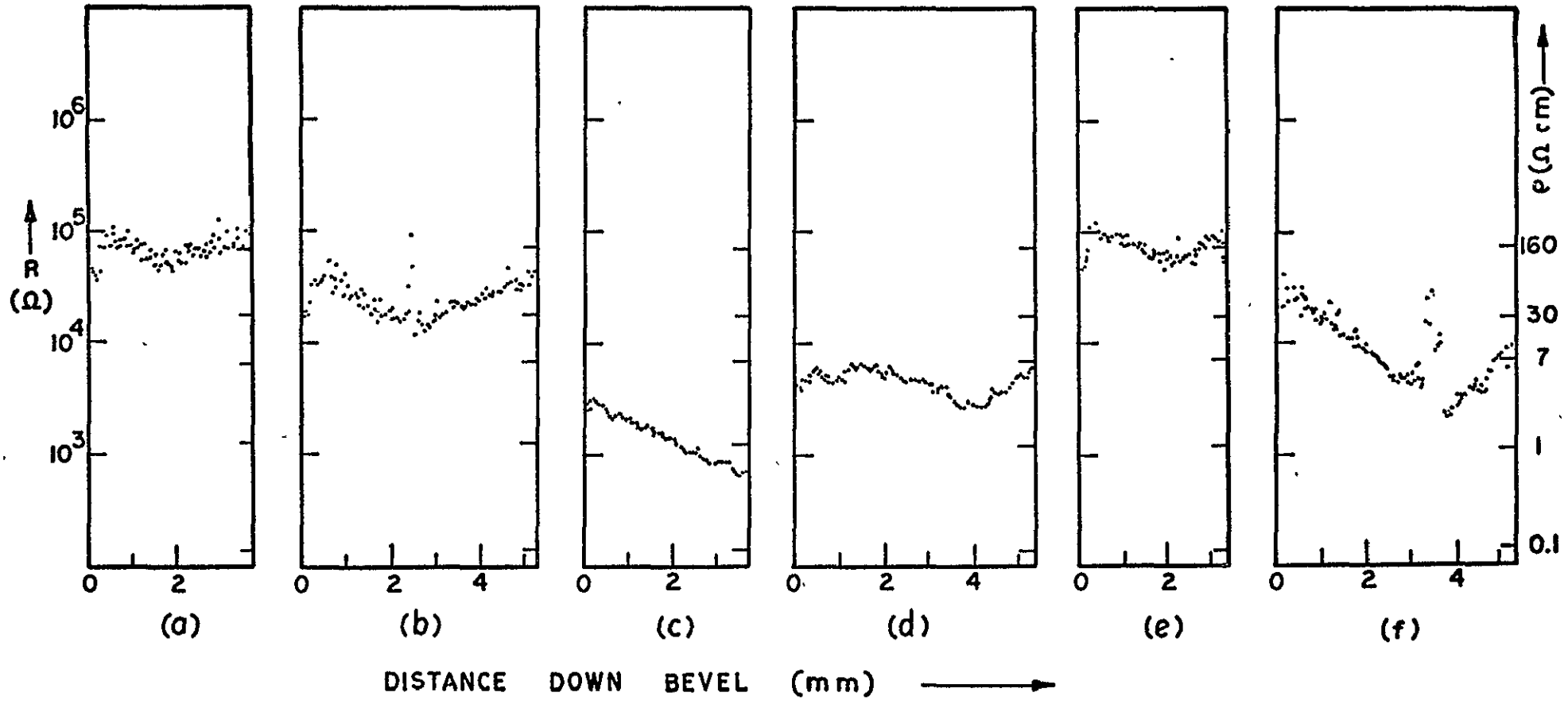
R (Ω)
10^6
10^5
10^4
10^3
ρ (Ω cm)
160
30
7
1
0.1
0
2
4
(a)
(b)
(c)
(d)
(e)
(f)
DISTANCE DOWN BEVEL (mm)

Fig. 4

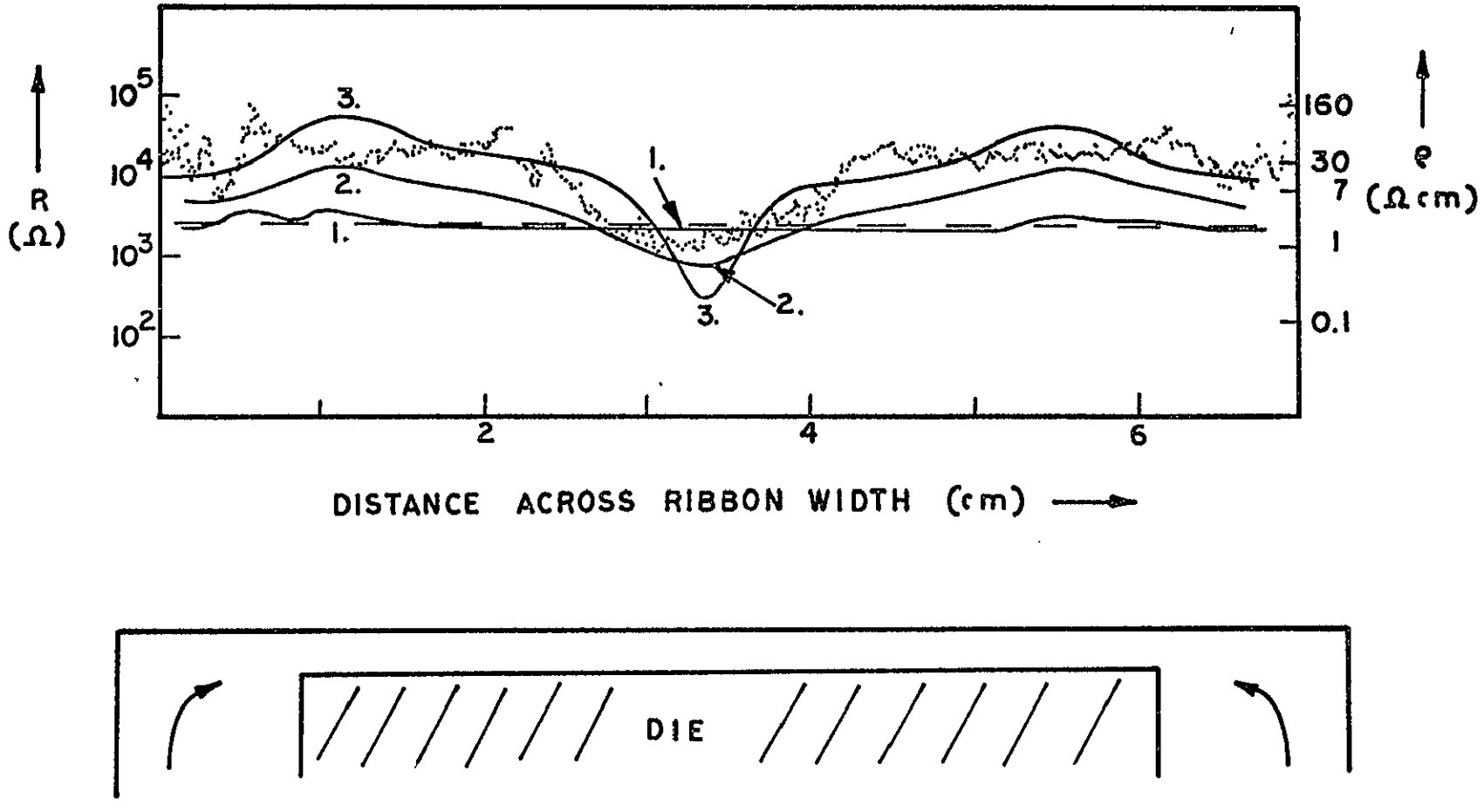
R
(Ω)
10^5
10^4
10^3
10^2
3.
2.
1.
160
30
7
1
0.1
ρ
(Ω cm)
2
4
6
DISTANCE ACROSS RIBBON WIDTH (cm)
DIE

Fig. 5

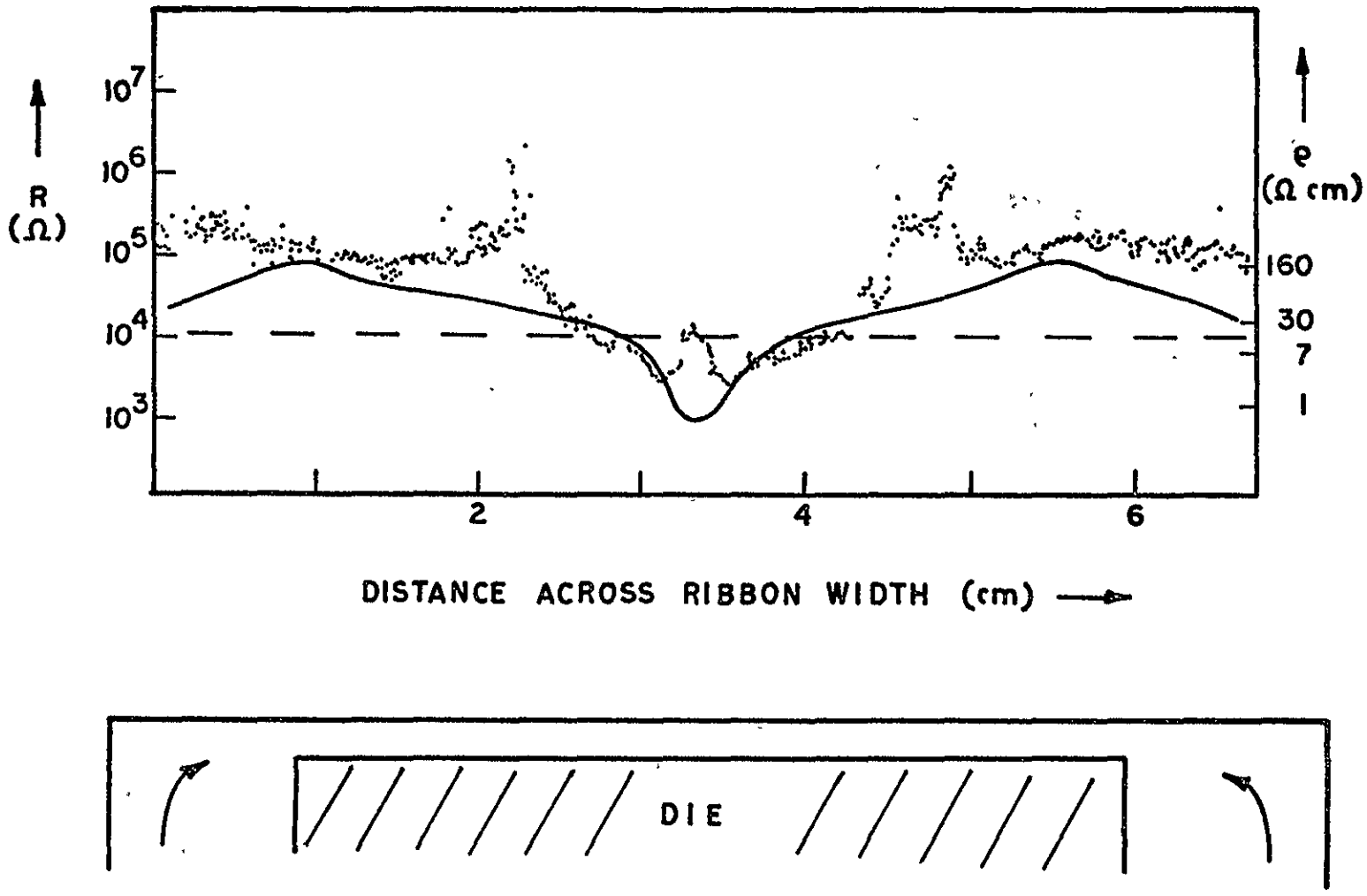
R
(Ω)
10^7
10^6
10^5
10^4
10^3
ρ
(Ω cm)
160
30
7
1
2
4
6
DISTANCE ACROSS RIBBON WIDTH (cm)
DIE

Fig. 6